geologica acta

Citation: Oliva-Urcia, B., Román-Berdiel, T., Torres-López, S., Villalaín, J.J., Casas-Sainz, A., 2025. Shortening-controlled magnetic fabrics in the Alpine thrust front of the Cantabrian Mountains. Geologica Acta, 23.25, 1-pgs. DOI: 10.1344/GeologicaActa2025.23.25

Online ISSN: 1696-5728

Shortening-controlled magnetic fabrics in the Alpine thrust front of the Cantabrian Mountains

Belén Oliva-Urcia[1] Teresa Román-Berdiel[1] Sara Torres-López[2] Juan José Villalaín[3] Antonio Casas-Sainz[1]

[1]**Geotransfer-IUCA, Departamento de Ciencias de la Tierra, Facultad de Ciencias, Universidad de Zaragoza**
C/ Pedro Cerbuna 12, Zaragoza, Spain, boliva@unizar.es; mtdjrb@unizar.es, acasas@unizar.es

[2]**Departamento de Geología y Geoquímica, Universidad Autónoma de Madrid**
Ciudad Universitaria de Cantoblanco, 28049 Madrid, Spain, sara.torres@uam.es

[3]**Dpto. Física, Universidad de Burgos, Escuela Politécnica Superior**
Avda. Cantabria s/n 09006, Burgos, Spain, villa@ubu.es

ABSTRACT

The magnetic fabrics (or anisotropy of magnetic susceptibility) are used in this work to decipher thrust kinematics in the Cantabrian (western) Pyrenees. Most of the analyzed rocks (total of 51 sites) correspond to the Mesozoic rifting and post-rifting stages (Triassic, Jurassic and Cretaceous) rocks in the Asturian-Leonese region, whose alpine structure is controlled by south-verging, basement-involved thrusts. Paramagnetic minerals are scarce as shown by the thermomagnetic analyses, and maghemite/hematite predominates as carriers of the magnetic fabric. The rifting phase is recorded by a primary fabric that remained unaltered during the alpine contraction, whereas the magnetic fabric of the Albian and Upper Cretaceous rocks show a reorientation due to contraction, which is better recorded in the fine grained continental facies of the Utrillas Group than in the carbonatic rocks overlying them. In the contractional fabrics found, the magnetic lineation delineates the thrust front enhancing the changes of the local shortening direction along. This reinforces the hypothesis of a strong control of the thrust direction by inherited structures.

KEYWORDS **Utrillas Group. Rift. Tectonic inversion. AMS.**

INTRODUCTION

The Mesozoic deposits in the Oviedo basin and at the South-Cantabrian Frontal Thrust represent the northernmost and westernmost outcrops of syn-rift deposits in Iberia that are related to the continental break-up at the start and during the Alpine cycle (Martín-Chivelet *et al.*, 2002) in the Iberian margin. The evidence of the rifting phases in northern Iberia are particularly important in the Basque-Cantabrian basin, with up to 5000m thick Aptian-Albian successions (Urgonian facies) (García-Mondéjar *et al.*, 1996). Conversely, the western part of the Cantabrian coast shows much thinner Mesozoic sequences, that together reach a maximum thickness of ca. 2500m.

The extensional models for the evolution of the Cantabrian mountains refer to poly-phased processes, strain localization and subsequent and/or stacking rift phases (Cadenas *et al.*, 2020 and references therein; Fig. 1). These authors indicate that in magma-poor and multi-stage

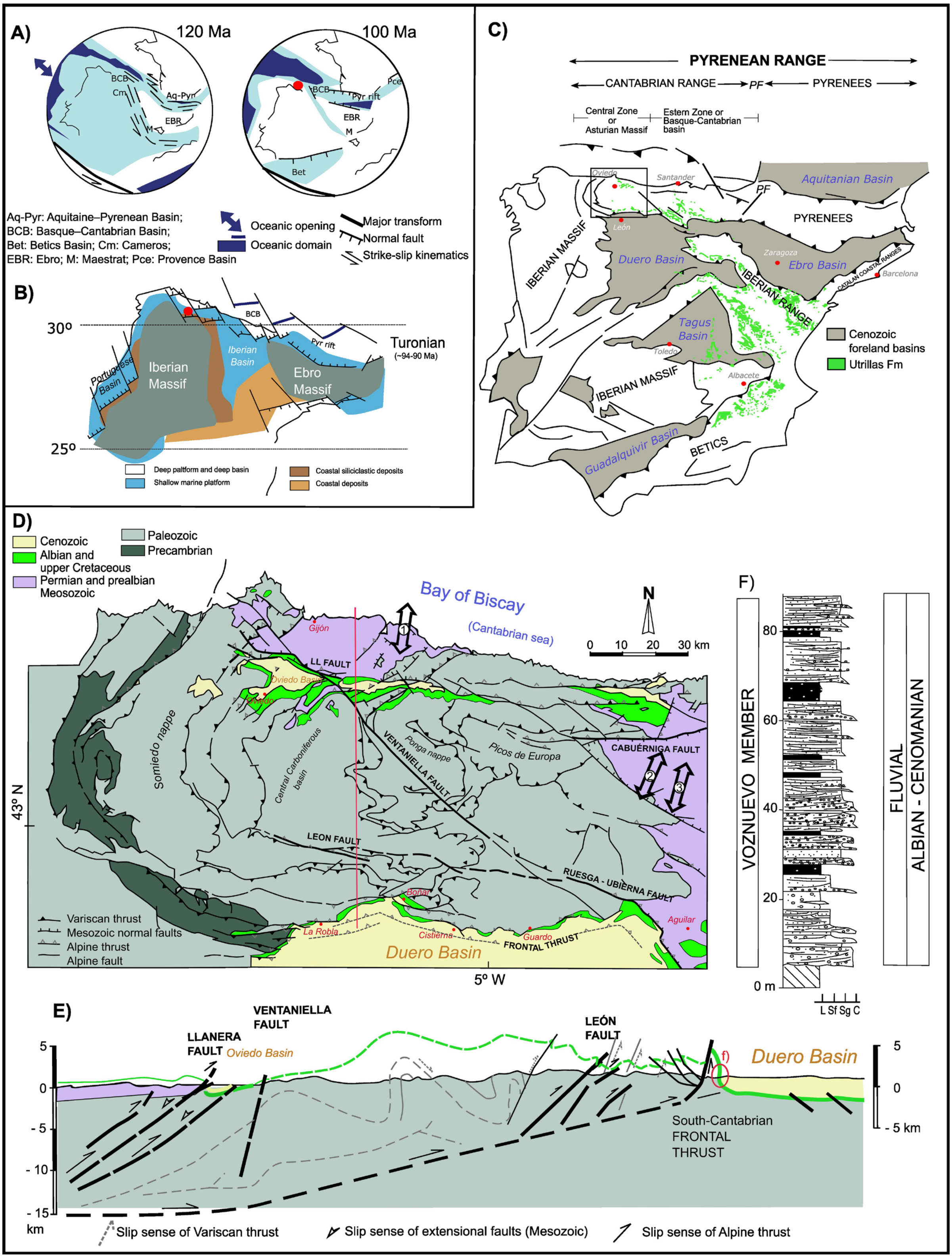

FIGURE 1. Paleogeographic reconstructions modified from A) Angrand *et al.* (2020) and B) Gil *et al.* (2006) from Aptian (~120Ma) to Turonian (~90Ma) times. Iberian and Ebro Massifs are emerged areas. Red dot: location of the study area. C) Location of the area in the general geological map of the Iberian Peninsula with Utrillas Group outcrops in green. PF: Pamplona Fault. Terms of geological sectors based on (Barnolas and Pujalte, 2004). D) Geological map of the area and E) cross-section showing the general structure (based on Alonso *et al*., 1996, 2007). F) The Voznuevo Mb. simplified from Herrero-Hernández and Gómez-Fernández (2012). Black arrows represent strain or stress of main extensional horizontal direction (Granado *et al*., 2018; Oliva-Urcia *et al*., 2013; Soto *et al*., 2008; Tavani and Muñoz, 2012).

rifted margins kinematics is difficult to study, specifically, the architecture of multi-stage rift systems and the control they exert on subsequent reactivation. They propose, for the Cantabrian area, the development of rifting in three stages: fault-bounded half-graben basins during the Triassic, a narrow deep transtensional system with pull-apart basins during the Late Jurassic to Barremian times and finally, during Aptian-Cenomanian times, a hyperextended system.

Magnetic fabrics have been proven useful for obtaining the main strain field, and when combined with fracture analyses, allow to reconstruct paleostresses, give a picture of the basinal history, both under extension and shortening, as exemplarized in marine syn-extensional deposits in the Apennines and in continental Plio-Pleistocene sediments of the Tiberian extensional basin (Alfonsi, 1997 and references therein). A revision of studies of magnetic fabric in tectonically inverted basins confirmed their applicability to reconstruct the extensional kinematics in areas where shortening is moderate (García-Lasanta *et al.*, 2018).

In this work we analyze the magnetic fabric of Mesozoic sediments, mostly in the continental Utrillas Group (~Albian-Cenomanian) sedimented at the end of the third rift phase in the Asturian-Leonese area (Cadenas *et al.*, 2020). The objective is twofold: on one side, to provide information about the extensional strain at the time of deposition, and on the other, to determine the areas where the tectonic inversion has modified the primary extensional fabric and can help to constrain the kinematic model of the area.

GEOLOGICAL SETTING

The study area is located in the central zone of the Cantabrian Range (or Asturian Massif), also known as the central part of the Astur-Galaica region (Martín-González and Heredia, 2011), to the west of the Basque-Cantabrian basin (Fig. 1C), considered as the western continuation of the Pyrenees (Capote *et al.*, 2002). The Mesozoic sediments deposited during the rifting phases fragmenting the basement massifs (Iberian and Ebro massifs in the Iberian microplate and the Armorican massif in the Eurasian plate) were subsequently incorporated into the Pyrenean Range during the alpine collision. These Mesozoic sediments remain undetached from the basement, in contrast to the Pyrenean isthmus (Alonso *et al.*, 1996). The general structure of the Cantabrian Range is interpreted as a monocline leading to a generalized uplift (at present 2500m.a.s.l.) due to a basement thrust along a shallow-dipping long ramp during alpine deformation (Alonso *et al.*, 1996). This main southward-verging thrust reactivated Variscan structures and can be related at depth with north-verging thrusts in the offshore of the Cantabrian margin (Álvarez-Marrón *et al.*, 1997; Pedreira *et al.*, 2015; Pedrera *et al.*, 2021). The total shortening during the tectonic inversion has been calculated at about 96km (Gallastegui, 2000) and occurred mostly during Late Eocene-Miocene times (Alonso *et al.*, 1996; Álvarez-Marrón *et al.*, 1997; Carriere, 2006; Gallastegui, 2000).

The foreland basin of the alpine Cantabrian ranges is the Duero Basin, that underwent a strong subsidence (ca. 1.5km) and was filled with terrestrial deposits (Herrero *et al.*, 2010). Meanwhile, the Oviedo Basin, located within the range (Fig. 1) is considered as a piggy-back basin after the inversion of the Llanera fault (Alonso *et al.*, 1996). Unconformities within the Cenozoic sediments indicate synsedimentary deformation in both the Oviedo and Duero basins. The Mesozoic cover is folded and verticalized to overturned due to basement thrusting, particularly in the southern Cantabrian front (Alonso *et al.*, 1996).

All the alpine shortening structure of the Cantabrian mountains is superimposed on Variscan and Late-Variscan structures that show a variety of geometries and behaviors (Alonso *et al.*, 1996; Llana-Fúnez and Marcos, 2007 among others). The Variscan cover (belonging to its external zones of the Iberian massif) comprises a thin series of Cambrian-Carboniferous rocks structured according to east-verging thrusts developed along long flats and short ramps. The post-Variscan series comprises Carboniferous and Permian, mostly sedimentary, rocks. The present-day, eastwards-concave, shape of the Variscan orogenic zone has been interpreted either as the result of a primary curvature or oroclinal bending (Gutiérrez-Alonso *et al.*, 2012; Pastor-Galán *et al.*, 2011; Weil *et al.*, 2000 and references therein).

The orientation of the alpine tectonic structures observed nowadays shows three main trends: E-W, NW-SE and NE-SW, inherited from the Variscan and post-Variscan structures (Fernández-Lozano *et al.*, 2019; González-Guerra, 2025; Heredia *et al.*, 2022). Larger E-W striking onshore faults are the Llanera, Ribadesella and León faults, cropping out in the same region with the long NW-SE striking Ventaniella fault, and a series of shorter NE-striking faults such as the Villaviciosa and Infiesto faults (Fig. 1), among others (more detail in the discussion section). The two main rifting stages occurred during Permian-Triassic and Late Jurassic times. The first rifting episode produced the deposit of alluvial detrital sediments and evaporites. During the second, main rifting episode (Late Jurassic-Early Cretaceous) graben and half-graben structures controlled sedimentation along the basin. An unconformity interpreted to happen in the Aptian due to sea level rise occurs, and a postrift sequence was deposited, starting with clastic deposits evolving to deeper facies in the Late Cretaceous (passive margin stage). The first evidences of shortening occurred in the Eocene in the offshore Asturian basin whereas unconformities in the Late Cretaceous-Paleocene are also interpreted as related to the inversion in other areas (Boillot *et al.*, 1979; Cadenas and Fernádez-Viejo, 2017; Cadenas *et al.*, 2020; Gallastegui, 2000; Granado *et al.*, 2018; Lepvrier and Martínez-García, 1990 and references therein). The Jurassic (about 1000m thick) in the northern part of the Oviedo basin has been the subject of structural and thermal studies that allow interpreting the age of fault activity during each particular time span. Temperatures did not exceed 200ºC (from vitrinite reflectance) and several stages of normal fracturing and thermal events are described (Suárez-Ruiz, 1988; Suárez-Ruiz and González Prado, 1995; Suárez-Ruiz *et al.*, 1996; Uzkeda *et al.*, 2025). In addition, an intra-Jurassic unconformity explained by continental uplift has been also described below the La Ñora/Vega Fms during the Early Kimmeridgian (Uzkeda *et al.*, 2016, 2025 and references therein).

Along the studied area, the Mesozoic crops out in two sectors. In the southern one, the Mesozoic is reduced to the Albian–Maastrichtian) and covers the basement in the foreland of the Cantabrian mountains. These outcrops are related to the South Cantabrian frontal thrust, between the Cantabrian mountains (Variscan Domain) and the Cenozoic deposits of the Duero Basin. In this area, the Upper Cretaceous succession unconformably overlies the Carboniferous rocks of the Cantabrian and Westasturian-Leonese zones and crops out along a 65km long, 5km wide narrow E-W band, which is the main object of this study (Herrero-Hernández and Gómez-Fernández, 2012).

In the northern sector of the studied zone, the Mesozoic crops out in a wider band, in the Oviedo basin (Fig. 1). Here, the Albian-Santonian interval is presently cropping out along an E-W band, of similar length to the previous one and overlies Paleozoic, Triassic and/or Jurassic rocks. The Albian-Upper Cretaceous sequence reaches a thickness of 150-650m and includes fluvial, transitional and shallow marine deposits. The detrital interval is equivalent to the Utrillas Sandstone (considered Group since Rodríguez-López (2008)), which are described as multicolored sandstones, intercalated with clays and conglomerates with rounded pebbles. All these materials are considered to be deposited in arid conditions (erg and arid braided system (Bueno-Cebollada *et al.*, 2023 and references therein). Locally, the detrital Albian-Upper Cretaceous unit is known as Voznuevo Member (Mb.) (or Pola de Siero Formation (Fm.) in the Oviedo Basin (González-Fernández *et al.*, 2004)).

Particularly in the Cantabrian mountains area, the Voznuevo Mb. (previously Fm.) is diachronous and represents a fluvial environment that evolves from a braided system in the West evolving to a meandering system towards the East, with paleocurrents suggesting a source area towards the SW (Jonker, 1972). The depositional environment has been later described as a delta fan, a delta dominated by tides or a tidal flat (Herrero-Hernández and Gómez-Fernández, 2012 and references therein, Fig. 1F). The siliciclastic Voznuevo Mb. cropping out along the South Cantabrian frontal thrust varies in thickness from 350 to 150m. Pollen data indicate that its upper part corresponds with the beginning of the Upper Cretaceous (Herrero-Hernández and Gómez-Fernández, 2012 and references therein). On top of it there is the Boñar Fm., consisting of limestones, dolostones, marls and sandstones, with a maximum thickness of 385m, that pinches out towards the West. The age of this unit has been inferred from lateral correlation with other units, determining that it expands from the Coniacian to the Maastrichtian (Herrero-Hernández and Gómez-Fernández, 2012 and references therein). In this area, the Cenozoic continental deposits of the endorheic foreland Duero basin unconformably overlie the Upper Cretaceous. They were sedimented in alluvial fan environments and reach 1.5–2km in thickness (Fig. 1E).

In the Oviedo Basin, north of the Llanera Fault, the Mesozoic is represented by the Permo-Triassic, (which overlies the pre-Variscan Paleozoic rocks), the Jurassic (only in the northern part) and the Albian-Upper Cretaceous (~300m in thickness) (Bernárdez, 2005; González-Fernández *et al.*, 2004). Permo-Triassic/Jurassic boundary has been dated with palinomorph taxa (Barrón *et al.*, 2006; López-Gómez *et al.*, 2019). The Cenozoic reaches 400m in thickness and overlies the Upper Cretaceous (Alonso *et al.*, 1996)

METHODOLOGY

A total of 677 samples distributed in 51 sites were analyzed with the aim of obtaining their magnetic fabrics. Among them, 37 sites belong to the Utrillas/Voznuevo units (red, fine grained silts and claystones), two were taken in Triassic rocks (Buntsandstein facies), six in Jurassic rocks (Lower and Upper Jurassic), five sites in Upper Cretaceous rocks and one site in Paleogene rocks. They are distributed in the northern part of the Duero foreland basin (37 sites) and around the Oviedo basin (14 sites), Table I Appendix, Figure 2.

In order to obtain fine grained sedimentary rocks, which are best suited for magnetic fabric analysis, hand samples of different sizes (from 1cm to 20cm edge) were oriented in the field with a magnetic compass. A total of 561 samples were originated from the hand samples and 116 from drill cores, using a battery powered drill machine refrigerated with water and oriented with a clinometer.

The magnetic fabrics of 12 sites were measured using a KLY3 and the rest of them using a KLY5A (AGICO Inc.) at the magnetic fabrics laboratory of the University of Zaragoza.

The magnetic susceptibility measures the capacity of a material of being magnetized while a weak magnetic field is applied. The anisotropic behaviour of the magnetic susceptibility (magnetic fabric) can also be described in terms of the susceptibility ellipsoid or the magnitude ellipsoid. This property provides information about the orientation distribution of mineral grains (Aubourg *et al.*, 1995; Borradaile, 1987; Borradaile, 1988; Borradaile and Jackson, 2004, 2010; Debacker *et al.*, 2004; Tarling and Hrouda, 1993). A second rank tensor represents the ellipsoid. Magnetic parameters of the magnetic ellipsoid were calculated using Anisoft 5 (Chadima *et al.*, 2020) based on Jelink (1981). They include the mean magnetic susceptibility (K_m), the magnetic lineation L (k_{max}/k_{min}) and the magnetic foliation, F (k_{int}/k_{min}) parameters (as in the Flinn diagram for strain), the corrected anisotropy degree Pj and the shape parameter T (oblate for values between 0 and 1 and prolate for values between -1 and 0). The direction of the magnetic lineation is the same of the maximum susceptibility (k_{max} axes) and the magnetic foliation is perpendicular to the minimum susceptibility direction (k_{min} axes) (Hrouda, 1982).

The orientation distribution of the k_{max} axes respect to bedding (the reference structural plane) and to the regional strike provides information about the development of the magnetic fabric and the related strain.

Thermomagnetic curves (temperature dependent magnetic susceptibility) were analyzed using a KLY3-CS, in Argon atmosphere for 29 samples (~0.5g) in order to obtain information about the carriers of the magnetic fabric. One sample in Triassic rocks, two in Jurassic rocks, three in Upper Cretaceous and the rest of the samples (23) in the Utrillas Group/Voznuevo Mb. Cureval 8 (Chadima and Hrouda, 2009) was the software used to represent data and calculate the paramagnetic contribution (hyperbolic decay of the magnetic susceptibility at low temperatures -room temperature to ~400ºC), calculate the alteration or visualize the decay temperature indicative of a ferromagnetic mineral.

RESULTS

Scalar parameters

The magnetic susceptibility varies from 461 to 3.5·e-6SI, with an average of 102·e-6SI (standard deviation of 77.6·e-6SI) without considering PLA 01 because of its abnormally high values (Tables 1; 2; II; Fig. 3A, B).

Grouping the samples by age and separating the Utrillas Group samples, the averaged values show the lower susceptibility for the Upper Cretaceous (limestones and marls of marine origin) and the Paleogene (one site only) and the higher values for the Utrillas Group (mostly red silts and clays). All sites show a magnetic Foliation (F) better defined than the Lineation (L), and the corrected anisotropy of the ellipsoid varies from smaller values in the Upper Cretaceous and the Jurassic to the higher values in the Triassic (clayish red beds). The shape parameter is oblate for all samples except for the site in the Paleogene (matrix in a conglomerate) with the larger values for the Triassic (older rocks, Table 2; Fig. 3).

In 15 sites the magnetic susceptibility has been normalized by mass in order to better constraint the value of Km. The standard procedure when measuring the magnetic fabric (AMS) in magnetic samples is to normalize the measurement by volume, using 10cm³ as a standard value. Since samples have different volumes, the measurement of the magnetic susceptibility is later normalized by the mass. Figure 4 shows the relationship between the values of the magnetic susceptibility normalized by volume (standard 10cm³) and the value after normalization by mass, and how the samples with more mass have larger values of Km when is normalized by volume (graph on the right).

It has been determined that the magnetic susceptibility of small unoriented samples (chips) provides good information of the anisotropy of the magnetic susceptibility

TABLE 1. Average and standard deviation values for all data: Km (mean susceptibility value), L: kmax/kmin; F: kint/kmin, Pj: corrected anisotropy degree and T: shape parameter (Jelinek, 1981).

	K_m	L	F	Pj	T
N	662	677	677	677	677
Mean	102 · e-6 SI	1.009	1.022	1.031	0.332
Standard deviation	7.7 · e-6 SI	0.025	0.029	0.032	0.413

FIGURE 2. Outcrops of the Triassic (PLA33), Jurassic (PLA40), Upper Cretaceous (pla16) and the Utrillas Group.

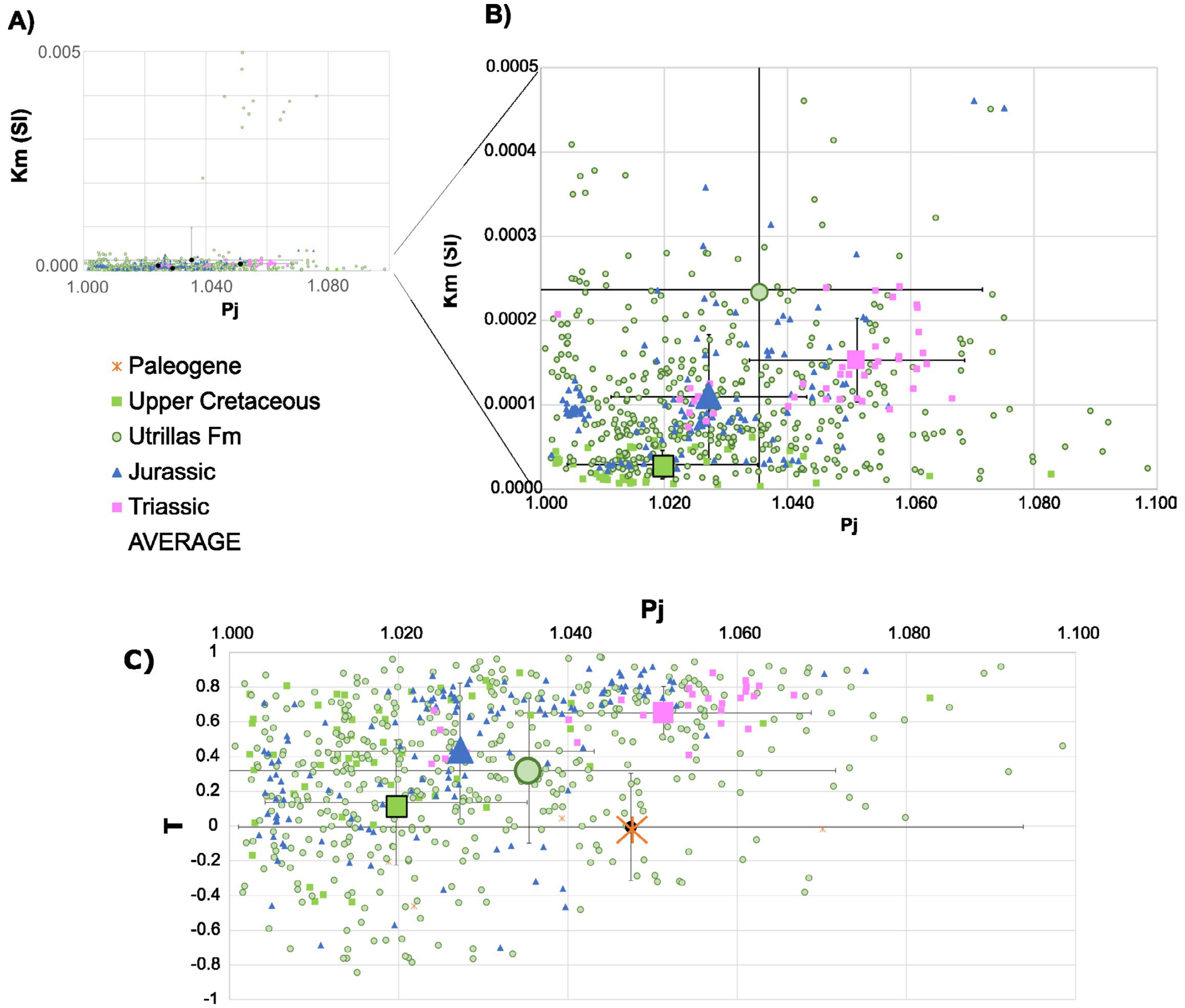

FIGURE 3. Parameters of the magnetic ellipsoid: magnetic susceptibility (Km), Pj (3A and enlarged in 3B) and Pj-T in 3C) for all the 677 samples and the averaged value by age (and Utrillas Group samples), the latter shown with larger symbols and standard deviations.

TABLE 2. Average and standard deviation values in the different units (and Utrillas Group): Km (mean susceptibility value), L: k_{max}/k_{min}; F: k_{int}/k_{min}, Pj: corrected anisotropy degree and T: shape parameter (Jelinek, 1981)

	K_m		L		F		Pj		T	
	Average	St. deviation	Average	St. deviation	Average	St. deviation	Average	St. deviation	Average	St. deviation
Paleogene	-5.09 E -06	3.61 E -06	1.019	0.013	1.026	0.033	1.047	0.046	-0.006	0.309
Up. Cretaceous	29.0 E -06	4.96 E -05	1.008	0.008	1.011	0.010	1.020	0.015	0.136	0.360
Utrillas Group	237 E -06	7.41 E -04	1.009	0.009	1.024	0.028	1.035	0.036	0.318	0.417
Jurassic	109 E -06	7.38 E -05	1.006	0.005	1.020	0.014	1.027	0.016	0.431	0.393
Triassic	153 E -06	4.96 E -05	1.007	0.003	1.040	0.015	1.051	0.017	0.652	0.152

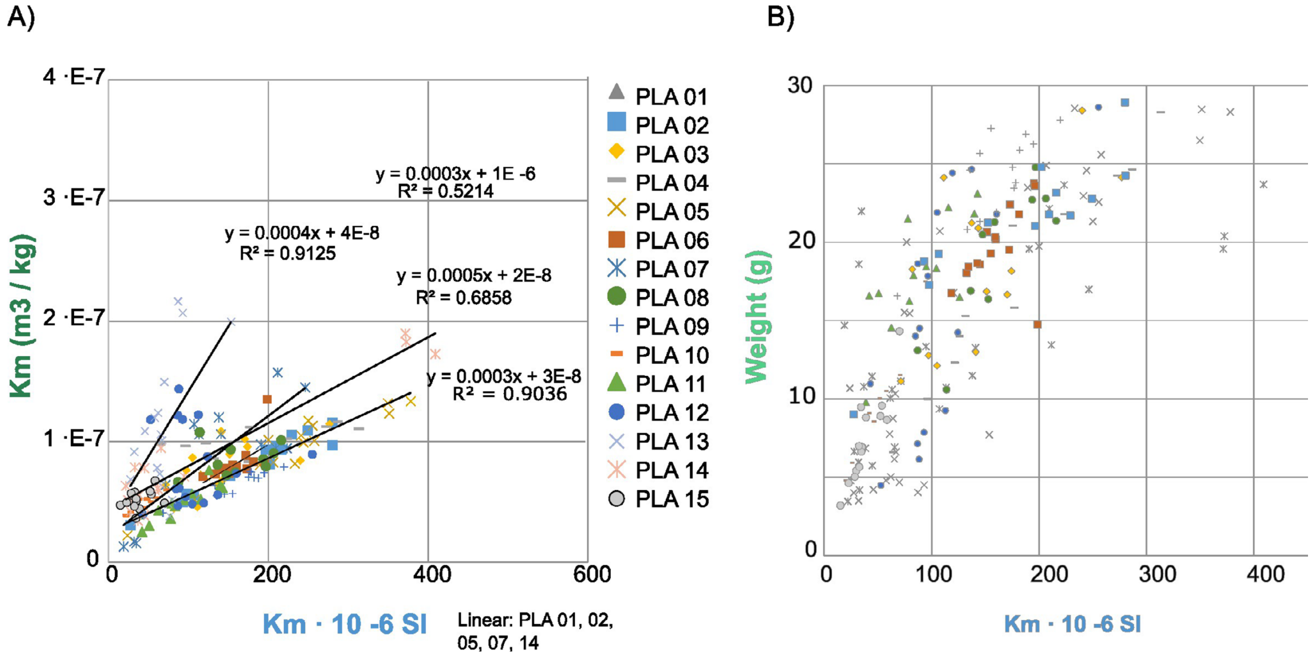

FIGURE 4. A) Magnetic susceptibility values normalized by mass for 15 sites. The correlation coefficient varies from 0.3 to 0.9 (some examples shown on the left). PLA 01 samples are out of the graph because of their larger values (correlation is shown). B) Variation of the magnetic susceptibility with weight.

in terms of scalar parameters in clays with low magnetite content (Gracia-Puzo *et al.*, 2021).

Magnetic carriers

The thermomagnetic curves of the temperature dependent magnetic susceptibility (k-T curves) are grouped depending on their behavior. Triassic, Jurassic and Upper Cretaceous show a similar variation: the curves are irreversible, with much higher susceptibility on the cooling curve (Fig. 5). This is due to new formation of magnetic phases during the experiment, which produces a higher susceptibility values in the cooling run. The new formation of a magnetic phase during heating occurs above 450ºC. The numerical characterization of this alteration during the proceeding has been calculated using the index A_{40} (Hrouda, 2003), which is called the alteration index (A_{40}= 100 (k_{40}-K_{40})/K_{40}; being k_{40} the magnetic susceptibility at 40ºC during cooling and K_{40} the magnetic susceptibility at 40ºC during heating). This author states that a positive A_{40} index indicates higher susceptibilities during cooling than during heating, while a negative value indicates the opposite relationship. For the older rocks and for those of the Upper Cretaceous, the A_{40} shows positive values (as expected from the observation of the k-T curves). Very large positive values were also obtained: ~6000 for BON04 -Up. Cret., ~1500 for PLA33 -Triassic- or ~370 for PLA40 -Jurassic-.

The decay temperature in the heating run indicates the presence of hematite for the Triassic (680ºC) and generally magnetite (~580ºC). One Jurassic sample (PLA36) shows a higher final temperature (maghemite/hematite). A similar behavior is obtained in the Utrillas Group in PLA18, which is irreversible and shows the final decay temperature of the heating run higher than 650ºC (maghemite/hematite). The paramagnetic contribution is almost null or very low (no hyperbolic decay of the heating run in the lower temperatures).

In other samples of the Utrillas Group there is more variability. Some samples are reversible for samples with very low magnetic susceptibility (BON11, PLA15, PLA13, PLA02) but also for a sample with higher magnetic susceptibility (PLA07). In these cases, A_{40} is very small (positive and negative values): -4 (PLA13), 0 (PLA02) or 36 (PLA15). There is some formation on new phases during heating, and three samples show a paramagnetic hyperbolic decay on the heating run (from 150ºC (PLA02) or 300ºC onwards (in BON11, PLA15…). The final decay on the heating run is closer to hematite temperature (675ºC).

The sample PLA 01, the one showing the highest susceptibility, shows a constant decay until reaching a magnetite temperature final decay in the heating run, with a reversible part between 500-700ºC (A_{40} is 45). The

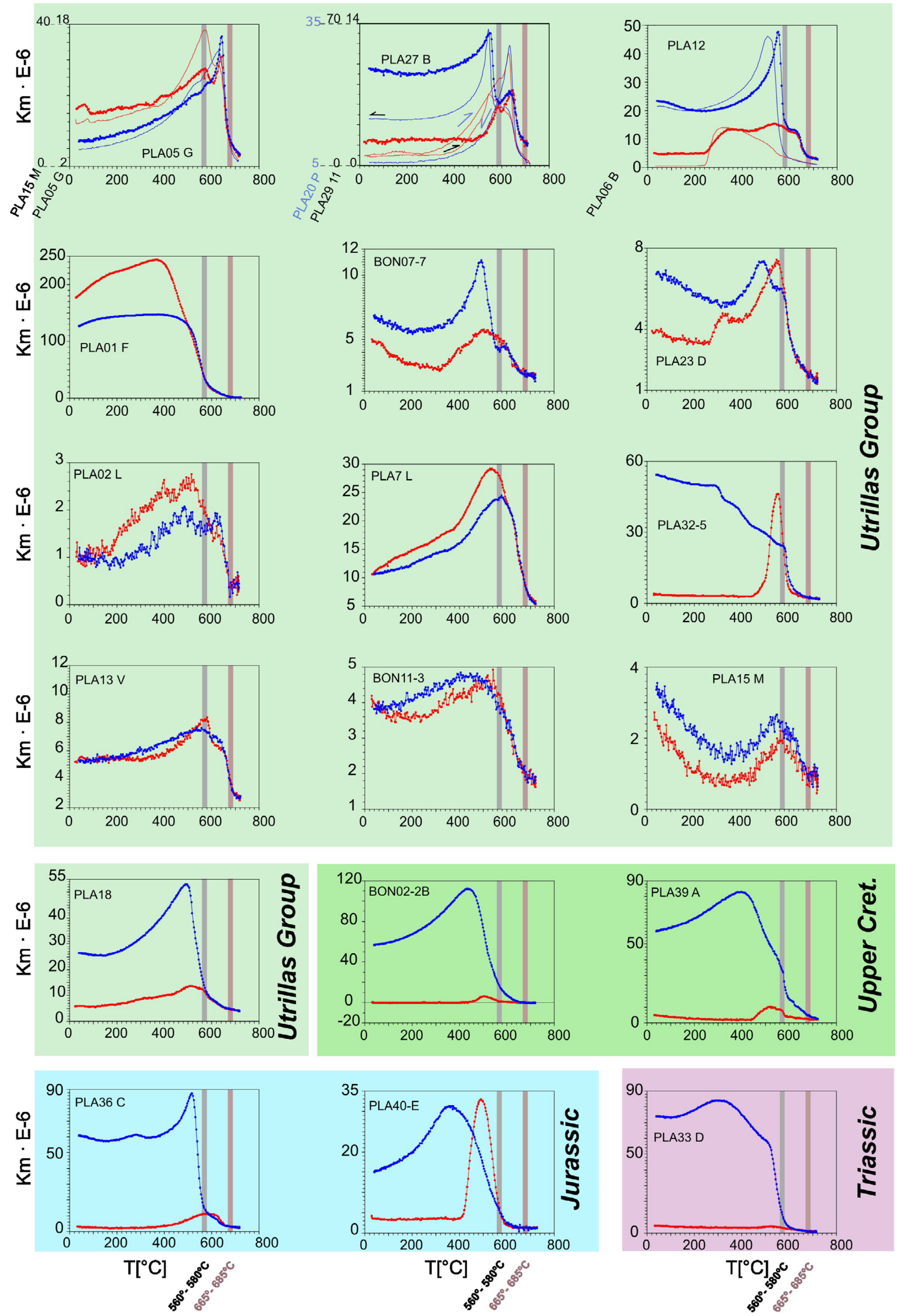

FIGURE 5. Temperature-dependent magnetic susceptibility of selected samples, heating run is in red, cooling run in blue. Background colour refers to rock type (age or Fm.). Colour bands that run vertically mark the temperature decay of magnetite (560-580ºC) and hematite (665-685ºC) for reference. At the top, several samples showing similar behavior are represented together.

heating run of the BON07 sample is similar to PLA15, BON11 or PLA13, but in BON07 the cooling curve shows two steps, suggesting two magnetic phases (one closer to a magnetite temperature and one closer to the maghemite/hematite temperature) and a contribution of paramagnetic minerals (~90% according to Cureval 8). Finally, eight samples of the Utrillas Group show some similarities (PLA15, PLA05, PLA27, PLA20, PLA29, PLA06, PLA12, PLA23); for example, they show two (or three) magnetic phases during heating, magnetite and hematite in PLA15, PLA05, PLA27, PLA20 and PLA29; the cooling run has higher susceptibility and a Hopkinson peak appears (in few samples also in the heating run). PLA12, PLA06 and PLA23 show these same two behaviors in the cooling run (hematite and magnetite) but the heating run shows new formation of a magnetic phase after 250ºC. Despite their similar behavior, the alteration index have different values: PLA06, PLA29 with values of 420 or even 65000, and PLA 20 (-19), reaching values of -44 in PLA05.

As a summary, in the sampled rocks, and particularly in the Utrillas Group, the ferromagnetic phase (or phases) predominate over the paramagnetic signal.

Orientation of the magnetic ellipsoid

The orientation of the magnetic ellipsoid is presented by sectors: i) Oviedo Basin (Fig. 6) and ii) Thrust front of the Cantabrian Range (Fig. 7) after bedding restored to horizontal (Table 3). In Table III the average for every site is shown.

In the Oviedo Basin, all subsectors cluster well when bedding is restored to the horizontal. The k_{min} axes cluster around the pole to bedding and the inclination of the average is higher than 85º for the Triassic, Jurassic and Upper Cretaceous rocks and 70º for the average of the Utrillas Group sites (Table 2). The k_{max} axes are oriented in a N-S direction for all rocks except for the Utrillas Group

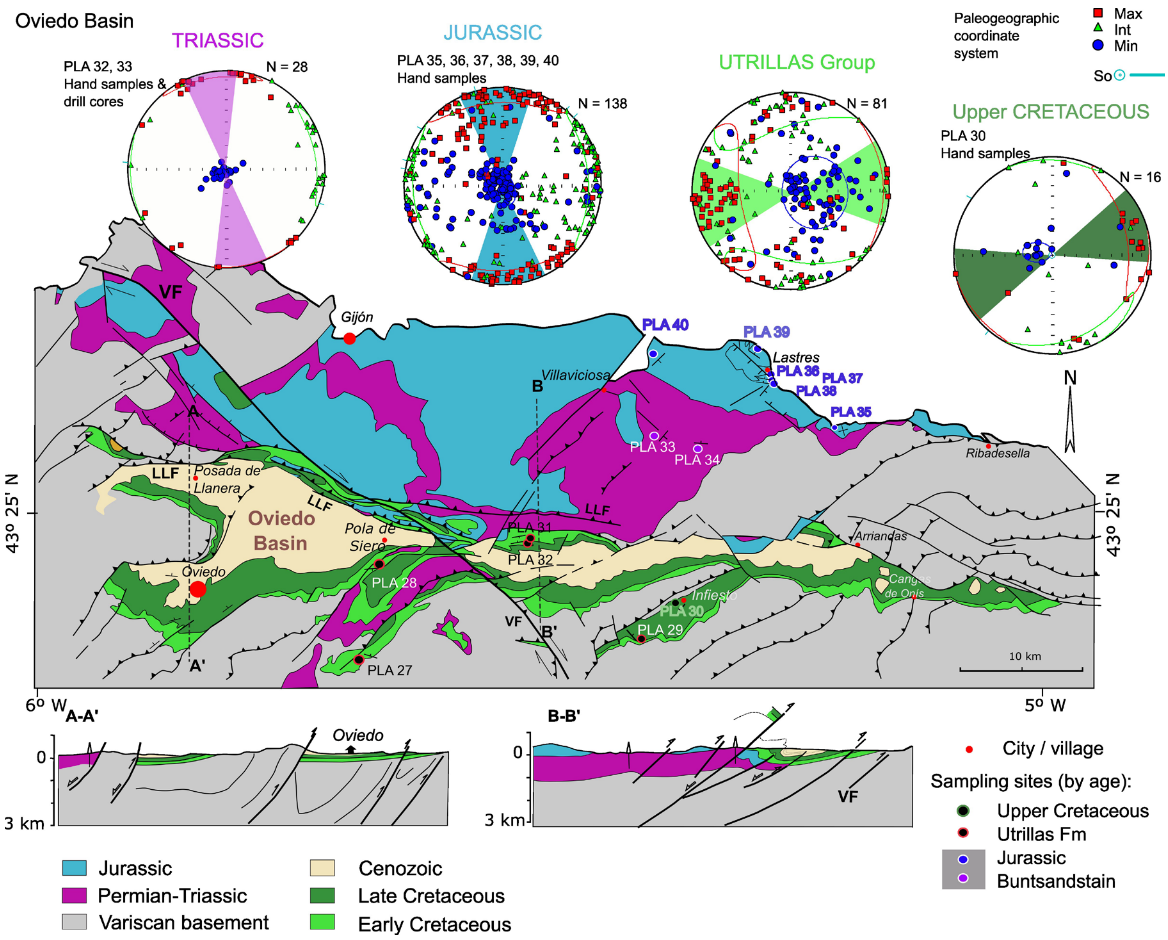

FIGURE 6. Stereoplots (Schmidt net, lower hemisphere) of the magnetic ellipsoid in the Oviedo Basin sector after bedding is restored to horizontal. Red squares: k_{max} axes, green triangles: kint axes, blue circles: kmin axes. Background colours in the stereoplots represent lithologies (age) and mark the orientation of k_{max} axes. Map and cross-sections simplified from (Alonso *et al.*, 1996), LLF: Llanera Fault, VF: Ventaniella Fault.

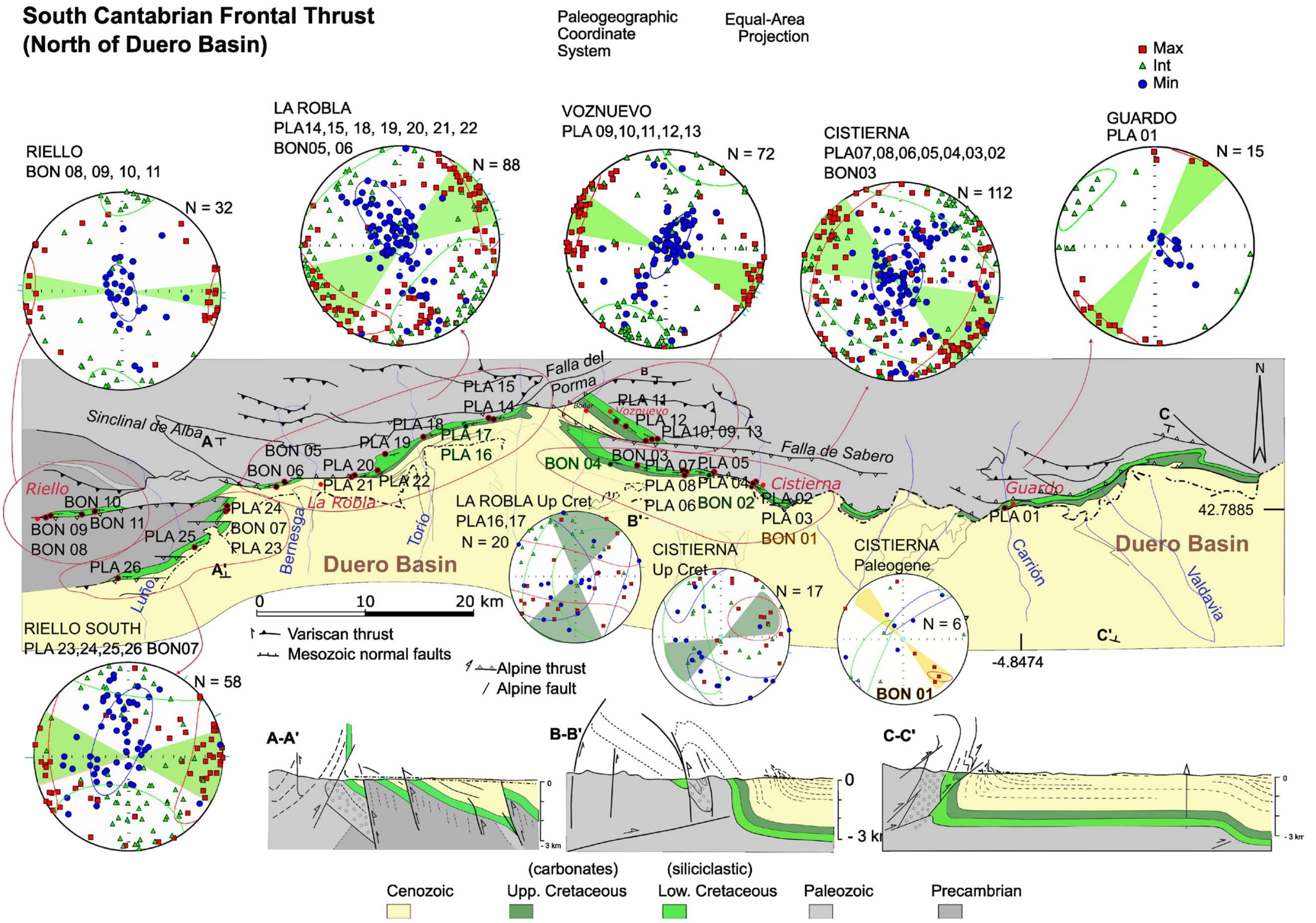

FIGURE 7. Stereoplots in lower hemisphere of the magnetic ellipsoid in the thrust front of the Cantabrian mountains (northern part of the Duero basin) after bedding is restored to horizontal. Red squares: k_{max} axes, green triangles: k_{int} axes, blue circles: k_{min} axes. Background colours in the stereoplots represent lithostratigraphic units (age) and mark the orientation of kmax axes as in Figure 6, plus the Paleogene in yellow. Map and cross-sections simplified from (Alonso *et al.*, 1996).

and one site of the Upper Cretaceous, that are oriented approximately with an E-W direction.

The sites in the Northern sector of the Duero Basin have been grouped by proximity and common orientation of the direction of regional outcrop, naming the subsectors according to the near villages (see map in Fig. 7). The Upper Cretaceous sites show the most scattered axes. The Paleogene shows a good clustering of the magnetic lineation (clustering of k_{max} axes) despite the fact the k_{min} axes are not clustered around the pole to bedding. The general orientation of the k_{max} axes of the Utrillas Group are E-W, WNW-ESE and ENE-WSW except for La Robla and Guardo subsectors, with a NE-SW orientation. In all the Utrillas Group sites the k_{min} axes are around the bedding pole, with some scattering on a girdle, on a vertical plane with a direction perpendicular to the k_{max} axes orientation (Fig. 7).

In any case, the larger scattering considering the Utrillas Group is in Riello South (confidence angles: 50/20, 5 sites), followed by similar values in La Robla (37/16, 9 sites), Voznuevo (30/10, 5 sites), Cistierna (27/21, 8 sites) and Riello (24/10, 4 sites).

DISCUSSION

The magnetic carrier of the anisotropy of magnetic susceptibility (magnetic fabric) according to the thermomagnetic curves, is maghemite/hematite for the Triassic and some Jurassic rocks, since the final decay is over 620ºC (Dunlop and Özdemir, n.d., 1997). In other marls and limestones of the Jurassic and Upper Cretaceous there is magnetite (decay at 580ºC). The procedure creates hematite in some cases since the cooling run has a higher temperature (Dunlop and Özdemir, 1997). The

TABLE 3. Average of the orientation of the magnetic ellipsoids grouped depending on age or formation and sectors with different orientation. Km: magnetic susceptibility, $K_{max\ (int,\ min)}$, dec: declination of the $K_{max\ (int,\ min)}$ after bedding restored to horizontal, $K_{max\ (int,\ min)}$ inc: inclination of the $K_{max\ (int,\ min)}$ after bedding restored to horizontal, con elip: confidence ellipse for the average. All calculations are from Anisoft5. See stereoplots in Figure 6

	Age/Fm.	SITES	Km (SI)	K_{max} dec	K_{max} inc	con elip	K_{int} dec	K_{int} inc	con elip	K_{min} dec	K_{min} inc	con elip
Oviedo Basin	Buntsandstein	PLA 33, 34	1.53 E-04	351	3	32//4	81	4	32//6	221	85	6//4
	Jurassic	PLA 35, 36, 37, 38, 39, 40	1.09 E-04	356	1	45//16	86	2	45//12	252	88	17//11
	Up. Cret	PLA30	4.66 E-05	71	11	47//11	162	6	47//8	282	77	12//8
	Utrillas Group	PLA 27, 28, 29, 31,32	6.20 E-05	263	21	54//27	354	4	54//30	94	70	9//8
South Cantarbian Frontal Thrust	Riello (Utrillas Group)	BON 08, 09, 10, 11	8.60 E-05	274	1	17//12	4	2	24//15	160	88	24//10
	Riello South (Utrillas Group)	PLA 23, 24, 25, 26, BON 07	1.09 E-04	96	9	46//26	189	14	50//43	333	73	50//20
	La Robla (Utrillas Group)	PLA 14, 15, 18, 19, 20, 21, 22 BON 05, 06	8.40E+01	231	6	46//17	138	26	47//35	334	64	37//16
	La Robla (Up. Cret.)	PLA 16, 17	2.10 E-05	11	2	69//57	103	46	74//66	277	44	74//56
	Voznuevo (Utrillas Group)	PLA 09, 10, 11, 12, 13	9.70 E-05	293	4	25//10	203	4	30//25	64	85	30//10
	Cistierna (Utrillas Group)	BON 03, PLA 07, 08, 06, 05, 04, 02, 03	1.60 E-04	122	5	53//22	212	2	53//26	326	85	27/21
	Cistierna (Up. Cret.)	BON 02, 04	2.23 E-05	62	42	34//24	268	46	72//27	163	13	72//24
	Cistierna (Paleogene)	BON 01	-5.00 E-06	135	20	18//5	243	39	54//15	25	43	54//9
	Guardo (Utrillas Group)	PLA 01	4.10E-03	241	5	25//6	305	13	26//13	103	76	15//5

Utrillas Group samples show more complex behavior, with the presence of magnetite and hematite revealed in the heating run. In any case, there are a majority of samples where no paramagnetic carrier can be inferred, except for BON07 or PLA15 where there is a hyperbolic decay during heating, indicating the presence of paramagnetic minerals. Therefore, ferromagnetic minerals are mostly the carriers of AMS.

The orientation of the magnetic ellipsoid in tectonically inverted basins, particularly the magnetic lineation (clustered k_{max} axes), has been used for reconstructing extensional strain at the time of basin development. The correlation was proposed by Mattei *et al.* (1997) based on that the magnetic lineation in weakly deformed marine clays follows the stretching lineation in an extensional basin. This observation has been transferred to other tectonically inverted basins and sediments. In general, it works when the carriers of the magnetic fabric are mostly clays or hematite, that is, platy minerals. In addition, depending on the type of the basin and its evolution, the primary extensional tectonic fabric can be masked or completely obliterated (see revision by García-Lasanta *et al.*, 2018 and references therein).

For the magnetic lineation to be used as stretching direction in rocks with scarce strain markers, two conditions need to be met. The first one is that k_{max} axes are located on the bedding plane, and therefore the k_{min} axes are at the pole of the bedding plane; the second one is that they are clustered. In addition, a general geological setting needs to be known in order to determine if the magnetic fabric development has continued during the inversion of the basin, and therefore, the first original information is lost.

In the studied area, some of the structures active during the Mesozoic and the Cenozoic are structures inherited from the Variscan and Late-Variscan stages (Alonso *et al.*, 1996; Granado *et al.*, 2018; Fernández-Lozano *et al.*, 2019; Heredia *et al.*, 2022; Uzkeda *et al.*, 2025). In general, E-W, NE-SW and NW-SE structures characterize the structural configuration in the area, particularly in its northern sector. According to previous authors, the E-W structures were extensional faults during the Permian-Triassic and Kimmeridgian rifting stages, and they were reactivated as reverse faults during the Cenozoic (Alpine inversion). Other Mesozoic normal faults, striking NE-SW and NW-SE, were reactivated as strike slip faults during the tectonic inversion (Cenozoic), showing dextral movement (the ones oriented NW-SE, such as the Ventaniella Fault), and sinistral the ones oriented NE-SW (as the Infiesto or the Villaviciosa faults) (Uzkeda *et al.*, 2016 and references therein). The Mesozoic structures are also inherited from previous Variscan and Late-Variscan structures (Heredia *et al.*, 2022 and references therein). The paleostress analyses in the Jurassic of the Oviedo Basin reveal a NNW-SSE horizontal s_1 (vertical s_3 or s_2) Lepvrier and Martínez-García (1990), which have been corroborated and completed by other authors who also inferred N-S tectonic transport (both extensional and contractional) (Granado *et al.*, 2018; Uzkeda *et al.*, 2016). A general N-S extension direction is obtained in the northern part, although orientation of extensional faults varies, probably due to previous anisotropies in the basement, as mentioned in earlier investigations (Gonzalo-Guerra, 2025; Heredia *et al.*, 2022; Lepvrier and Martínez-García, 1990; Uzkeda *et al.*, 2016). Therefore, the extensional and contraction transport direction are roughly N-S, which suggest that the magnetic fabric of the Triassic and Jurassic sites records the information of these extensional events, whereas the Utrillas Group rocks reveal the contractional event, perpendicular to main E-W faults (such as the Llanera fault).

The Utrillas Group, which has been sampled at both sides of the Ventaniella Fault, and the Upper Cretaceous site, have a ~E-W orientation of the magnetic lineation (clustered k_{max} axes), Figure 8. This can be interpreted either as a result of the Cenozoic stage (shortening fabrics) or as fabrics formed during the rotational movement of Iberia (left-lateral transtension, see Asti *et al.*, 2022). However, there are not data enough to confirm one of these hypotheses.

In the neighborhood of the southern Cantabrian Frontal Thrust there is no previous available information about paleostress orientations. Nevertheless, the existing geological maps allow us to reliably establish the relationship between the macro-structure and the magnetic fabrics. We here discuss the orientation of the magnetic lineation of the Utrillas Group respect to the structures and regional and local strike of beds. A good parallelism is observed between the orientation of the magnetic lineation and the structure, particularly when the regional strike coincides with tectonic structures (thrusts) in orientation as in the Riello or Cistierna sectors. In South Riello, the magnetic lineation follows the regional trend (oriented N090E), and in La Robla and Voznuevo the magnetic lineation also follows the strike of bedding. In Guardo, the magnetic lineation of the only sampled site is oblique with respect to the regional structure (ca. 50º). The Upper Cretaceous sites also show an oblique magnetic lineation with respect to the regional structure, although the k_{max} axes are very scattered. The Paleogene site near Cistierna shows a magnetic lineation slightly oblique with respect to the regional structures (Fig. 8E). In general, the magnetic lineation of the Utrillas Group delineates the structure, exhibiting a curved pattern at the thrust front.

Considering orientations at site level (Fig. 9), the sites that exhibit a "parallel" (up to 30º difference) averaged K_{max} axes with the strike of bedding plane are the majority. The

DOI: 10.1344/GeologicaActa2025.23.25

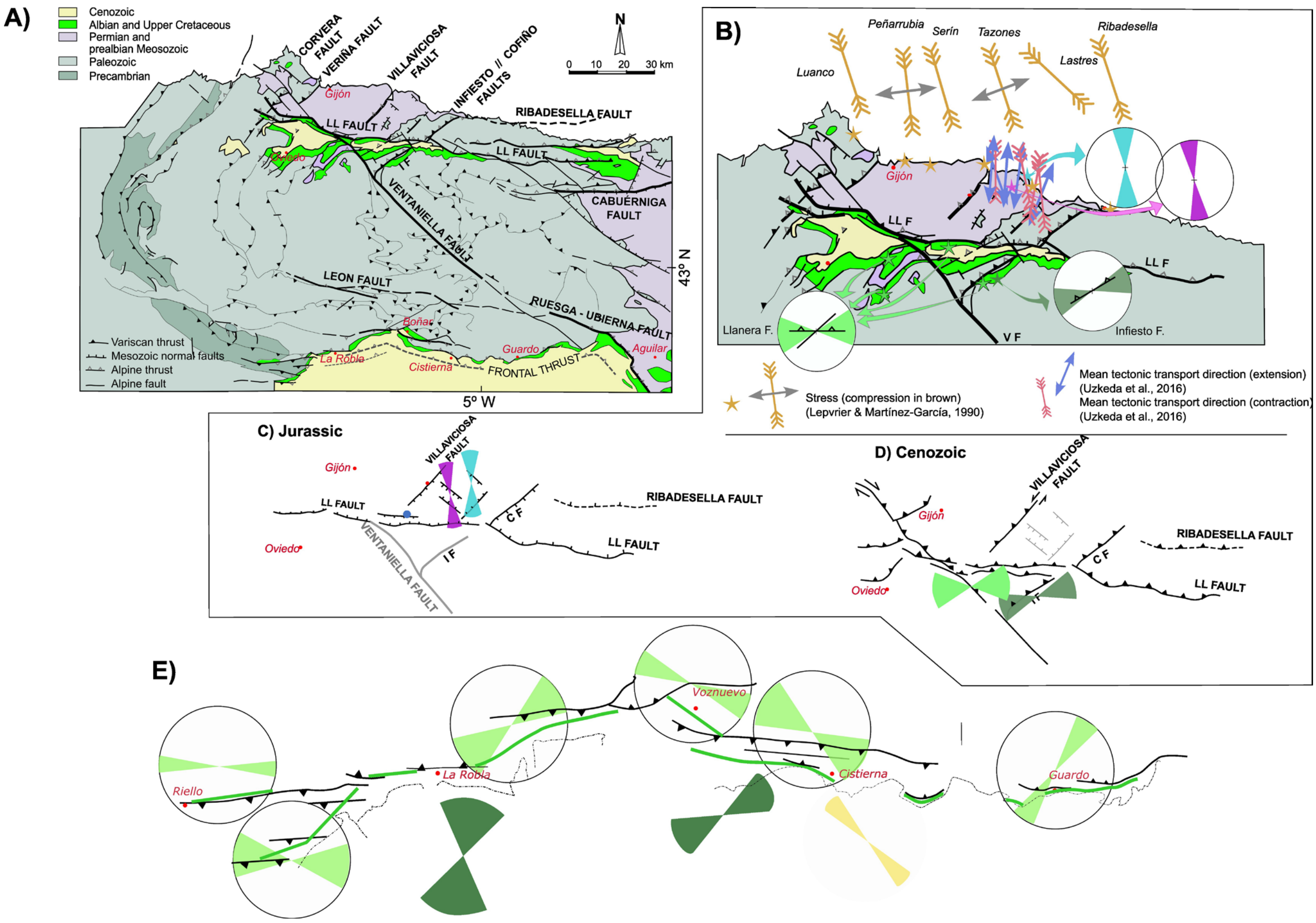

FIGURE 8. A) Summary of faults in the general geologic map. B) The northern sector shows paleostress information from previous authors (Granado *et al.*, 2018; Lepvrier and Martínez-García, 1990; Uzkeda *et al.*, 2025) and the orientation of the clustered k_{max} axes. C, D) At different stages during the evolution of the basin and its inversion (reference of faults from Uzkeda *et al.*, 2025). E) Summary of the magnetic lineation and regional structures for the South Cantabrian frontal thrust. Colours in magnetic lineation indicate age as follows, pink: Triassic, blue: Jurassic, light green: Utrillas Group, dark green: Upper Cretaceous, yellow: Paleogene. There are three magnetic lineations without external circle to indicate the lower quality of the magnetic lineation (either by dispersion or because the k_{min} axes are not perpendicular to bedding).

sites with the most oblique orientation of the average K_{max} axes respect to the strike of the bedding are located near i) Riello South, ii) one site in La Robla -East- (PLA14), four sites near Cistierna. However, if we consider the Jurassic and Triassic outcrops, their magnetic lineation is mostly oriented perpendicular to the significant (extensional) structures such as Llanera faults. Sites PLA03, 05, 14, 21, 26 of the Utrillas Group and BON4 of the Upper Cretaceous are located along the South Cantabrian Frontal Thrust.

Therefore, we can consider a twofold model for the evolution of magnetic fabrics in Mesozoic rocks, according to the age of rocks and their basinal evolution. In the case of the Albian claystones and siltstones, the magnetic lineation in most sites is parallel to the strike of beds, closely associated with the basement thrusting and inversion structures. We interpret that their origin responds to shortening. The scattering or slight deviations from the strike of bedding could be associated with a former extensional fabric, slightly oblique to this direction. On the contrary, the Triassic-Jurassic sites show a N-S orientation of the magnetic lineation, and are well grouped, suggesting that they developed during the extension and were not modified during the inversion (Fig. 10), otherwise, the k_{max} axes would be grouped in an E-W direction. This agrees also with a different basinal history that would allow to create well-developed magnetic fabrics associated with the normal faults. The post-rift Utrillas Group., instead did not develop such a strong fabric, and either the sedimentary fabric or the

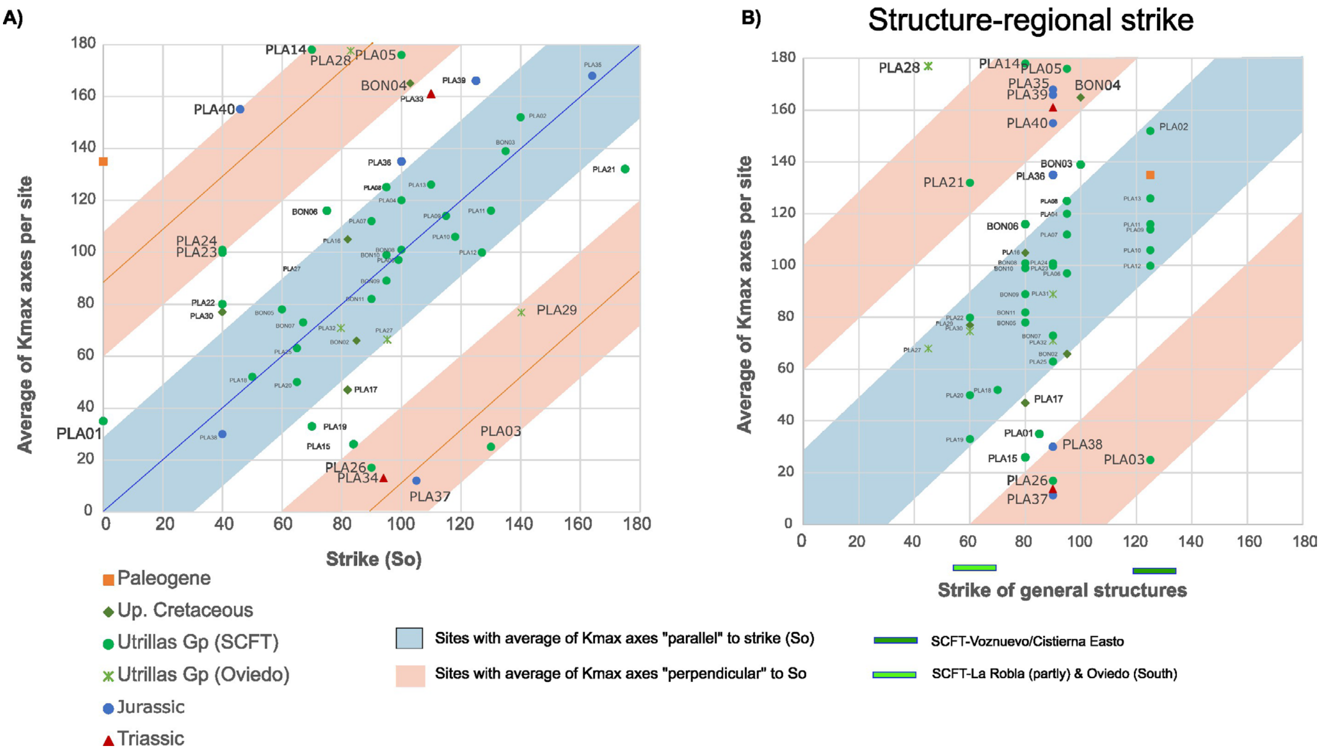

FIGURE 9. A) the average values of k_{max} declination and the strike of bedding. B) The average values of k_{max} declination and the strike of the general structure by sectors.

incipient exensional fabric were easily re-oriented by the shortening structures.

These new results confirm stress and stain analyses from previous works in the area and help constrain the kinematics related to the opening of the Bay of Biscay and the tectonic evolution of Iberian plate. As Angrand *et al.* (2020) and Asti *et al.* (2022) (and references therein) discussed, the Mesozoic kinematic evolution of the Iberian plate has been largely debated and different models have been developed since the seventies. Particularly, these authors indicate that the Mesozoic extension direction is difficult to estimate. As shown before, coeval Late Jurassic activity of E-W, NE-SW and NW-SE trending sets of normal faults reveal complex syn-rift kinematics, but a NNE-SSW direction of extension based on interpretation of joint set directions has been presented (Granado *et al.*, 2018; Uzkeda *et al.*, 2016). Our results of the magnetic fabric in Triassic and Jurassic rocks reveal a N-S direction of extension.

The development of the magnetic fabric in the rifting phases in the Permo-Triassic to Jurassic has its counterpart in the magnetic fabric developed in the red fine grained continental deposits of the post-rift depositional phase. In this case, the shortening features mask the original fabric, revealing a magnetic fabric that mimics the general structure, particularly the Southern Cantabrian Frontal Thrust (Fig. 10). In addition, the scattered K_{min} axes may indicate different degree in the strain underwent during the inversion, following the general model evolution of magnetic fabric with deformation (Parés *et al.*, 1999) (also it can be due to different methods in sampling, number of samples, etc).

CONCLUSIONS

The new results of the magnetic fabric of 51 sites (most of them from the Albian claystones and siltstones) in the southern Cantabrian thrust front and the Oviedo basin allows to characterize the orientation of strain axes both during the Mesozoic extension (20% of sites) and the Cenozoic shortening (80% of sites).The magnetic carriers are mainly ferromagnetic grains (mostly hematite in the red clays).

The combination with previous results obtained from paleostress analysis allows confirming that i) the magnetic fabric, oriented during the Mesozoic according to the extension direction related to rifting (Triassic and Jurassic) in the Bay of Biscay, at present shows a NNE-SSW

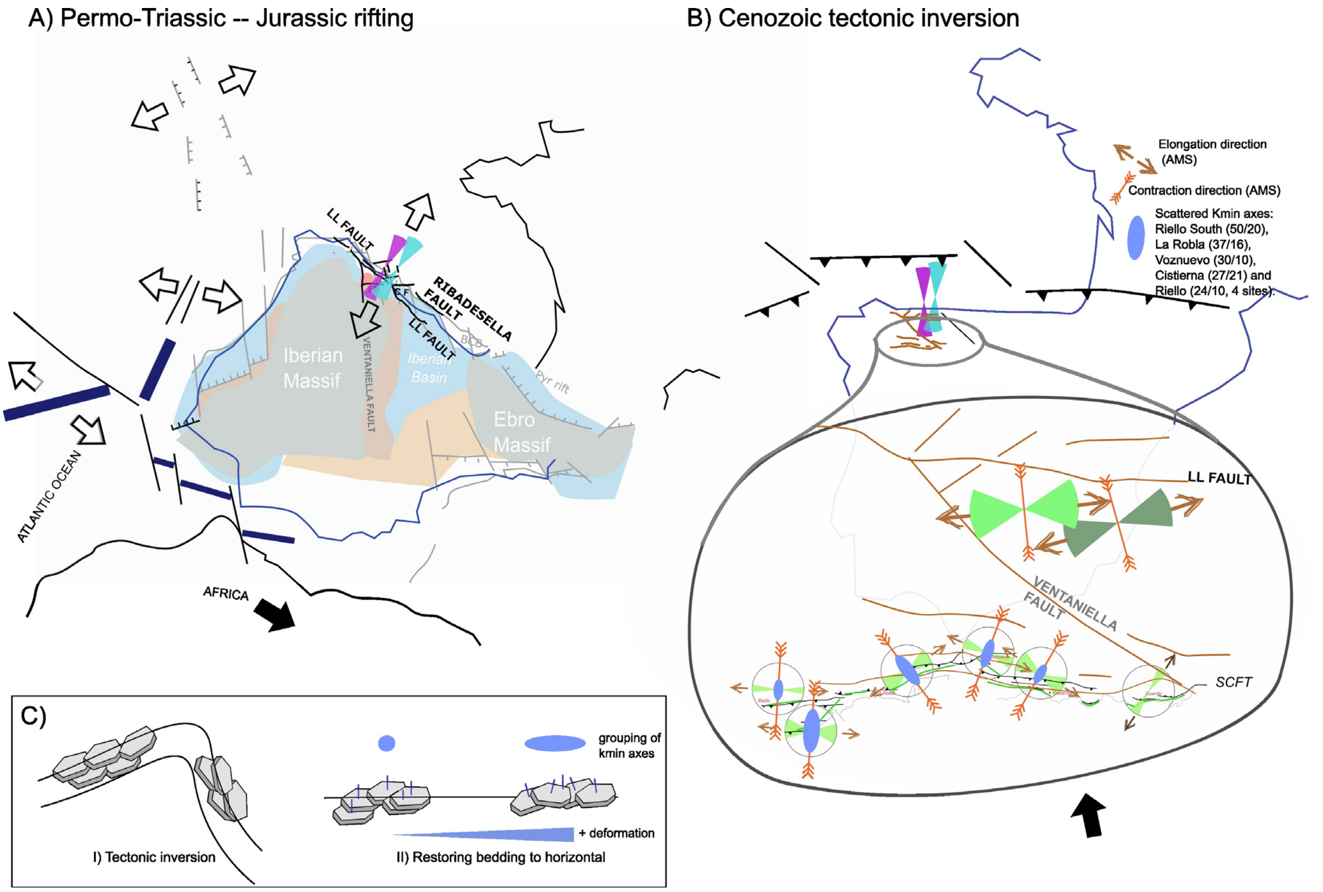

FIGURE 10. Reconstruction of strain considering the magnetic fabric data during A) the rifting phases and B) during the tectonic inversion. C) The more scattered k_{min} axes, the more deformation.

orientation, and remained unchanged after the tectonic inversion; ii) the tectonic inversion altered the (presumably weak) primary fabric in the Utrillas Group deposits, recorded only in a few sites, and created a new magnetic fabric that strictly delineates the thrust front, thus providing the local strain conditioned by inherited faults.

Respect to methodology we can conclude that magnetic fabric data provides useful information as long as sedimentary rocks are fine grained. Different sampling methodologies reinforce the magnetic fabric results.

ACKNOWLEDGMENTS

Project I+D+I research project PID2019-108753GB-C2 (C22 and C21) of the MICIN/AEI/10.13039/501100011033, by “ERDF A way of making Europe” and Project by Gobierno de Aragón (E32_23R: Geotransfer Research Group) are acknowledged. We also acknowledge the comments and suggestions of two Reviewers which improved the first version of the manuscript.

REFERENCES

Alfonsi, L., 1997. Paleomagnetic and anisotropy of magnetic susceptibility (AMS) analyses of the Plio-Pleistocene extensional Todi Basin, central Italy. Annals of Geophysics, 40(6).

Alonso, J.L., Pulgar, F.J.A., Pedreira, D., 2007. El relieve de la Cordillera Cantábrica. Enseñanza de las Ciencias de la Tierra, 1(2), 151-163.

Alonso, J.L., Pulgar, J.A., García-Ramos, J.C., Barba, P., 1996. W5 Tertiary basins and Alpine tectonics in the Cantabrian Mountains (NW Spain). In: Friend, P., Dabrio, C. (eds.). Tertiary basins of Spain: The stratigraphic record of crustal kinematics. 214-227.

Angrand, P., Mouthereau, F., Masini, E., Asti, R., 2020. A reconstruction of Iberia accounting for Western Tethys–North Atlantic kinematics since the late-Permian–Triassic. Solid Earth, 11(4), 1313-1332.

Asti, R., Saspiturry, N., Angrand, P., 2022. The Mesozoic Iberia-Eurasia diffuse plate boundary: A wide domain of distributed transtensional deformation progressively focusing along the North Pyrenean Zone. Earth Sciences Reviews, 230, 104040.

Aubourg, C., Rochette, P., Bergmüller, F., 1995. Composite magnetic fabric in weakly deformed black shales. Physics of the Earth and Planetary Interiors, 87(3), 267-278.

Álvarez-Marrón, J., Rubio, E., Torné, E., 1997. Subduction-related structures in the North Iberian margin. Journal of Geophysical Research: Solid Earth, 102(B10), 22497-22511.

Barnolas, A., Pujalte, V., 2004. Pirineos: Rasgos distintivos y subdivisión. In: Vera, J.A. (ed.). Geología de España. Madrid, SGE-IGME, 233-237.

Barrón, E., Gómez, J.J., Goy, A., Pieren, A.P., 2006. The Triassic–Jurassic boundary in Asturias (northern Spain): Palynological characterisation and facies. Review of Palaeobotany and Palynology, 138(3-4), 187-208.

Bernárdez, E., 2005. Discusión sobre la Revisión y síntesis litoestratigráfica del sector occidental de la cuenca cretácica de Asturias, Trabajos de Geología, 24, 43-80. Réplica por B. González Fernández, E. Menéndez Casares, M. Gutiérrez Claverol y J.C. García-Ramos. Trabajos de Geología, 25, 117-137.

Boillot, G., Dupeuble, P.A., Malod, J., 1979. Subduction and tectonics on the continental margin of northern Spain. Marine Geology, 35, 53-70.

Borradaile, G., 1987. Anisotropy of magnetic susceptibility: Rock composition versus strain. Tectonophysics, 138(2-4), 327-329.

Borradaile, G.J., 1988. Magnetic susceptibility, petrofabrics and strain. Tectonophysics, 156(1-2), 1-20. DOI: https://doi.org/10.1016/0040-1951(88)90279-X

Borradaile, G.J., Jackson, M., 2004. Anisotropy of magnetic susceptibility (AMS): Magnetic petrofabrics of deformed rocks. London, The Geological Society, 238(1, Special Publications), 299-360.

Borradaile, G.J., Jackson, M., 2010. Structural geology, petrofabrics and magnetic fabrics (AMS, AARM, AIRM). Journal of Structural Geology, 32(10), 1519-1551. DOI: https://doi.org/10.1016/j.jsg.2009.09.006

Bueno-Cebollada, C.A., de la Horra, R., Barrenechea, J.F., Meléndez, N., Barrón, N., Fregenal-Martínez, M., 2023. Mid-Albian to earliest Cenomanian climate cycles indicated by humid paleosols developed within the arid braidplain facies of the Utrillas Group of east-central Spain. Palaeogeography, Palaeoclimatology, Palaeoecology, 626, 111701. DOI: https://doi.org/10.1016/j.palaeo.2023.111701

Cadenas, P., Fernádez-Viejo, G., 2017. The Asturian Basin within the North Iberian margin (Bay of Biscay): Seismic characterisation of its geometry and its Mesozoic and Cenozoic cover. Basin Research, 29(4), 521-541.

Cadenas, P., Manatschal, G., Fernádez-Viejo, G., 2020. Unravelling the architecture and evolution of the inverted multi-stage North Iberian-Bay of Biscay rift. Gondwana Research, 88, 67-87.

Capote, R., Muñoz, J.A., Simón, J.L., Liesa, C.L., Arlegui, L.E., 2002. Alpine tectonics I: The Alpine System north of the Betic Cordillera. In: Gibbons, W., Moreno, T. (eds.). The Geology of Spain. London, The Geological Society, 385-397.

Carriere, K., 2006. Neoproterozoic to Holocene tectonothermal evolution of the southern Cantabrian Mountains NW Iberia, revealed by apatite fission-track thermochronology. PhD Thesis. Heidelberg (Germany), Ruprecht-Karls-Universität, 289pp.

Chadima, M., Hrouda, F., 2009. Cureval 8 [Computer software].

Chadima, M., Hrouda, F., Jelinek, V., 2020. Anisoft 5 [Computer software]. AGICO Inc.

Cifelli, F., Mattei, M., Chadima, M., Hirt, A.M., Hansen, A., 2005. The origin of tectonic lineation in extensional basins: Combined neutron texture and magnetic analyses on "undeformed" clays. Earth and Planetary Science Letters, 235(1), 62-78. 62-68.

De Vicente, G., Vegas, R., Muñoz-Martín, A., Van Wees, J. D., Casas-Sainz, A., Sopeña, A., Sánchez-Moya, Y., Arche, A., López-Gómez, J., Olaiz, A., Fernández-Lozano, J., 2009. Cambridge University Press.Tectonophysics271Tectonophysics307

Debacker, T.N., Robion, P., Sintubin, M., 2004. The anisotropy of magnetic susceptibility (AMS) in low-grade, cleaved pelitic rocks: Influence of cleavage/bedding angle and type and relative orientation of magnetic carriers. London, The Geological Society, 238(1, Special Publications), 77-107.

Dunlop, D., Özdemir, Ö., 1997. Rock magnetism: Fundamentals and frontiers. Cambridge University Press.

Dunlop, D., Özdemir, Ö. (n.d.). Dunlop, D. J., & Özdemir, Ö. (1997). Rock magnetism: Fundamentals and frontiers (No. 3). Cambride, Cambridge university press.

Fernández-Lozano, J., Gutiérrez-Alonso, G., Willingshofer, E., Sokoutis, D., De Vicente, G., Cloetingh, S., 2019. Shaping of intraplate mountain patterns: The Cantabrian orocline legacy in Alpine Iberia. Lithosphere, 11(5), 708-721.

Gallastegui, J., 2000. Estructura cortical de la cordillera y margen continental cantábricos: Perfiles ESCI-N. Trabajos de Geología, 22, 3-234.

García-Lasanta, C., Oliva-Urcia, B., Casas-Sainz, A.M., Román-Berdiel, T., Izquierdo-Llavall, E., Soto, R., Calvín, P., Mussaid, B., El Ouardi, H., Kullberg, J.C., Villalaín, J.J., 2018. Inversion tectonics and magnetic fabrics in Mesozoic basins of the Western Tethys: A review. Tectonophysics, 745, 1-23. DOI: https://doi.org/10.1016/j.tecto.2018.08.005

García-Mondéjar, J., Agirrezabala, L.M., Aranburu, A., Fernández-Mendiola, P., Gómez-Pérez, I., López-Horgue, M., Rosales, I., 1996. Aptian—Albian tectonic pattern of the Basque—Cantabrian Basin (Northern Spain). Geological Journal, 31(1), 13-45.

Gil, J., García-Hidalgo, J., Segura, M., Carenas, García, A., Temiño, J., Díaz de Neira, A., 2006. Stratigraphic architecture, palaeogeography and sea-level changes of a third order depositional sequence: The late Turonian–early Coniacian in the northern Iberian Ranges and Central System (Spain). Sedimentary Geology, 191(3-4), 191-225.

Gonzalo-Guerra, B., 2025. Superposición de estructuras Variscas y Alpinas en el entorno de los Picos de Europa, Sierra de Cuera y Escudo de Cabuérniga (Cordillera Cantábrica, NO de España). PhD Thesis. Oviedo (Spain), Universidad de Oviedo, 816pp.

González-Fernández, B., Menéndez-Casares, E., Gutiérrez-Claverol, M.A., 2004. Revisión y síntesis litoestratigráfica del sector occidental de la cuenca cretácica de Asturias. Trabajos de Geología, 24, 43-80.

Gracia-Puzo, F., Aubourg, C., Casas-Sainz, A., 2021. A fast way to estimate the clay fabric from shale fragments. Key example from a strained thrust footwall (Pyrenees). Journal of Structural Geology, 152, 104443.

Granado, P., Tavani, S., Carrera García de Cortázar, N., Muñoz, A., 2018. Deformation pattern around the Conejera fault blocks (Asturian basin, North Iberian Margin). Geologica Acta, 16(4), 357-373.

Gutiérrez-Alonso, G., Johnston, S.T., Weil, A.B., Pastor-Galán, D., Fernández-Suárez, J., 2012. Buckling an orogen: The Cantabrian Orocline. GSA Today, 22(7), 4-9.

Heredia, N., Martín-González, F., Farias, P., García-Sansegundo, J., Pedreira, D., Gonzalo-Guerra, B., García-Davia, G., Mateos, G., Flórez-Rodríguez, A.G., 2022. Geology of the Cabuérniga Fault System: evolution of a large Alpine strcutre with Variscan inheritance. Jorunal of Maps, 18(2), 168-177.

Herrero, A., Alonso-Gavilán, G., Colmenero, J.R., 2010. Depositional sequences in a foreland basin (north-western domain of the continental Duero basin, Spain). Sedimentary Geology, 223(3-4), 235-264.

Herrero-Hernández, A., Gómez-Fernández, F., 2012. Palaeoshoreline for the Late Cretaceous marine platform in the Iberian Trough (Leonese Area, Spain) deduced from outcrop and subsurface analysis. Cent. Eur. J. Geosciencies, 4(3), 395-415. DOI: https://doi.org/10.2478/s13533-011-0067-6

Hrouda, F., 1982. Magnetic anisotropy of rocks and its application in geology and geophysics. Geophysical Surveys, 5(1), 37-82. DOI: https://doi.org/10.1007/BF01450244

Hrouda, F., 2003. Indices for numerical characterization of the alteration processes of magnetic minerals taking place during investigation of temperature variation of magnetic susceptibility. Studia Geophysica et Geodaetica, 47, 847-861.

Jelinek, V., 1981. Characterization of the magnetic fabric of rocks. Tectonophysics, 79, 63-70.

Jonker, R.K., 1972. Fluvial sediments of Cretaceous age along the southern border of the Cantabrian Mountains, Spain. Leidse Geologische Mededelingen, 48(2), 275-379.

Lepvrier, C., Martínez-García, E., 1990. Fault development and stress evolution of the post-Hercynian Asturian Basin (Asturias and Cantabria, northwestern Spain). Tectonophysics, 184(3-4), 345-356.

Llana-Fúnez, S., Marcos, A., 2007. Convergence in a thermally softened thick crust: Variscan intracontinental tectonics in Iberian plate rocks. Terra Nova, 19(6), 393-400.

Martín-Chivelet, J., Berástegui, X., Rosales, I., Vilas, L., Vera, J.A., Caus, E., Gräfe, K.U., Mas, R., Puig, C., Segura, M., Robles, S., Floquet, M., Quesada, S., Ruiz-Ortiz, P.A., Fregenal-Martínez, M.A., Salas, R., Arias, C., García, A., Martín-Algarra, A., … Ortega, F., 2002. Cretaceous. In: Gibbons, W., Moreno, T. (eds.). The Geology of Spain. London, The Geological Society, 255-292.

Mattei, M., Sagnotti, L., Faccena, C., Funiciello, R., 1997. Magnetic fabric of weakly deformed clay-rich sediments in the Italian peninsula: Relationship with compressional and extensional tectonics. Tectonophysics, 271(1), 107-122.

Oliva-Urcia, B., Román-Berdiel, T., Casas, A.M., Bógalo, M.F., Osácar, M.C., García-Lasanta, C., 2013. Transition from extensional to compressional magnetic fabrics in the Cretaceous Cabuérniga basin (North Spain). Journal of Structural Geology, 46, 220-234.

Parés, J.M., van der Pluijm, B.A., Dinarés-Turell, J., 1999. Evolution of magnetic fabrics during incipient deformation of mudrocks (Pyrenees, northern Spain). Tectonophysics, 307(1-2), 1-14. DOI: https://doi.org/10.1016/S0040-1951(99)00115-8

Pastor-Galán, D., Gutiérrez-Alonso, G., Weil, A.B., 2011. Orocline timing through joint analysis: Insights from the Ibero-Armorican Arc. Tectonophysics, 507, 31-46. DOI: https://doi.org/10.1016/j.tecto.2011.05.005

Pedreira, D., Alfonso, J.C., Pulgar, J.A., Gallastegui, J., Carballo, A., Fernàndez, M., García-Castellanos, D., Jiménez-Munt, I., Semprich, J., García-Moreno, O., 2015. Geophysical-petrological modeling of the lithosphere beneath the Cantabrian Mountains and the North-Iberian margin: Geodynamic implications. Lithos, 230, 46-68.

Pedrera, A., García-Senz, J., Peropadre, C., Robador, A., López-Mir, B., Díaz-Alvarado, J., Rodríguez-Fernández, L.R., 2021. The Getxo crustal-scale cross-section: Testing tectonic models in the Bay of Biscay-Pyrenean rift system. Earth-Science Reviews, 212, 103429.

Rodríguez-López, J.P., 2008. Sedimentología y evolución del sistema desértico arenoso (erg) desarrollado en el margen occidental del Tethys durante el Cretácico Medio, Cordillera Ibérica. Provincias de Teruel y Zaragoza.

Soto, R., Casas-Sainz, A.M., Villalaín, J.J., Gil-Imaz, A., Fernández-González, G., Del Río, P., Calvo, M., Mochales, T., 2008. Characterizing the Mesozoic extension direction in the northern Iberian plate margin by anisotropy of magnetic susceptibility (AMS). Journal of the Geological Society, 165(6), 1007-1018.

Suárez-Ruiz, 1988. Caracterización, clasificación y estudio de la evolución de la materia orgánica dispersa (MOD) en el Jurásico de Asturias y Cantabria. PhD Thesis. Oviedo (Spain), Universidad de Oviedo, 372pp.

Suárez-Ruiz, I., Iglesias, M.J., Jiménez Bautista, A., Laggoun-Défarge, F., Prado, J.G., 2006. El azabache en Asturias: características físico-químicas, propiedades y génesis. Trabajos de Geología, 26, 9-18.

Suárez-Ruiz, I., González-Pardo, J., 1995. Characterization of Jurassic black sales from Asturias (northen Spain): evolution and petroleum potential. In: Snape, S. (ed.). Composition, Geochemistry and Conversion of Oil Shales. Dordrecht, Kluwer Academic Publishers, 387-393.

Tarling, D.H., Hrouda, F., 1993. Magnetic anisotropy of rocks. Springer Science & Business Media.

Tavani, S., Muñoz, J.A., 2012. Mesozoic rifting in the Basque–

Cantabrian Basin (Spain): Inherited faults, transversal structures and stress perturbation. Terra Nova, 24, 70-76.

Uzkeda, H., Bulnes, M., Poblet, J., García-Ramos, J.C., Piñuela, L., 2016. Jurassic extension and Cenozoic inversion tectonics in the Asturian Basin, NW Iberian Peninsula: 3D structural model and kinematic evolution. Journal of Structural Geology, 90, 157-176.

Uzkeda, H., Poblet, J., Bulnes, M., 2025. Late Triassic to present-day tectono-thermal history of the coastal part of the Asturian basin: Implications for hydrocarbon exploration and for the North-Iberian margin evolution. Marine and Petroleum Geology, 171, 107158.

Weil, A.B., Van der Voo, R., van der Pluijm, B.A., Parés, J.M., 2000. The formation of an orocline by multiphase deformation: A paleomagnetic investigation of the Cantabria-Asturias Arc (northern Spain). Journal of Structural Geology, 22, 735-756.

Manuscript May 2025;
revision accepted September 2025;
published Online November 2025.

APPENDIX I

TABLE I. Name, location, age, lithostratigraphic unit and bedding data of sampled sites, overturned bedding plane. With asterisk, information from Uzkeda *et al.* (2016)

Site	WGS84		Unit / Age			Bedding		
			Age - lithology			(Strike / Dip)		
BON01	42.80594	-5.136878		Paleogene	Red fine grain matrix in conglomerate	0	0	
BON02	42.81248	-5.18359	Santonian - Campanian	Up. Cretaceous	White limestones	85	38	N (i)
BON03	42.8183	-5.26409	Utrillas Group	Albian-Cenomanian	Red clays	105	50	S
BON04	42.82025	-5.295666	Overlaying Utrillas Group	Up. Cretaceous	White sandy limestones	103	37	S
BON05	42.80215	-5.66475	Utrillas Group	Albian-Cenomanian	Red sand	60	90	
BON06	42.80059	-5.671615	Utrillas Group	Albian-Cenomanian	Red clay	75	75	N (i)
BON07	42.78134	-5.731408	Utrillas Group	Albian-Cenomanian	Red sand	67	38	S
BON08	42.77585	-5.930607	Utrillas Group	Albian-Cenomanian	Red, grey clay	90	38	S
BON09	42.77611	-5.931068	Utrillas Group	Albian-Cenomanian	Red clay	90	38	S
BON10	42.77854	-5.895338	Utrillas Group	Albian-Cenomanian	Red sand	95	30	S
BON11	42.77893	-5.880925	Utrillas Group	Albian-Cenomanian	Red sand	90	55	S
PLA01	42.77879	-4.859867	Utrillas Group	Albian-Cenomanian	Red sand, clays	0	0	
PLA02	42.80627	-5.135779	Utrillas Group	Albian-Cenomanian	Red clays	140	64	N (i)
PLA03	42.80593	-5.136353	Utrillas Group	Albian-Cenomanian	Red clays	130	56	N (i)
PLA04	42.81381	-5.182706	Utrillas Group	Albian-Cenomanian	Red clays	100	26	N (i)
PLA05	42.81413	-5.182364	Utrillas Group	Albian-Cenomanian	Red clays	100	26	N (i)
PLA06	42.81363	-5.209984	Utrillas Group	Albian-Cenomanian	Red lutites	99	80	S

TABLE I. Continued

Site	WGS84		Unit / Age		Age - lithology	Bedding (Strike / Dip)		
PLA07	42.81532	-5.210937	Utrillas Group	Albian-Cenomanian	Red fine grained sand	90	80	S
PLA08	42.81498	-5.2115	Utrillas Group	Albian-Cenomanian	Clays, lutites	99	80	S
PLA09	42.84249	-5.25638	Utrillas Group	Albian-Cenomanian	Red clays	115	25	S
PLA10	42.84207	-5.259379	Utrillas Group	Albian-Cenomanian	Red, grey clay	118	21	S
PLA11	42.85451	-5.290982	Utrillas Group	Albian-Cenomanian	Red fine grained sand	130	16	S
PLA12	42.84975	-5.278611	Utrillas Group	Albian-Cenomanian	Red fine grained sand	127	16	S
PLA13	42.84399	-5.254374	Utrillas Group	Albian-Cenomanian	Red, yellow limolite	110	28	S
PLA14	42.85953	-5.429666	Utrillas Group	Albian-Cenomanian	fine grained sand	70	70	N (i)
PLA15	42.85862	-5.428313	Utrillas Group	Albian-Cenomanian	fine grained sand	84	65	N (i)
PLA16	42.85165	-5.457595	overlaying Utrillas Group	Up. Cretaceous	Grey limestones	82	80	N (i)
PLA17	42.85175	-5.457572	overlaying Utrillas Group	Up. Cretaceous	Grey marls	82	80	N (i)
PLA18	42.84446	-5.50323	Utrillas Group	Albian-Cenomanian	Red fine grained sand	60	85	S (i)
PLA19	42.82851	-5.547434	Utrillas Group	Albian-Cenomanian	Red lutites	75	62	S
PLA20	42.80862	-5.587336	Utrillas Group	Albian-Cenomanian	Red lutites	65	57	N (i)
PLA21	42.80811	-5.587309	Utrillas Group	Albian-Cenomanian	Red lutites	65	57	N (i)
PLA22	42.81347	-5.561612	Utrillas Group	Albian-Cenomanian	Red sandy	45	50	W (i)
PLA23	42.78018	-5.731339	Utrillas Group	Albian-Cenomanian	Red lutites	40	20	SE
PLA24	42.78584	-5.732215	Utrillas Group	Albian-Cenomanian	Red lutites	40	20	SE
PLA25	42.75062	-5.765395	Utrillas Group	Albian-Cenomanian	Red sand	65	26	SE

TABLE I. Continued

Site	WGS84		Unit / Age	Age - lithology		Bedding (Strike / Dip)		
PLA26	42.72463	-5.879773	Utrillas Group	Albian-Cenomanian	Red lutites	90	87	S
PLA27	43.29709	-5.700914	Utrillas Group	Albian-Cenomanian	Red sand	107	29	N
PLA28	43.37812	-5.665957	Utrillas Group	Albian-Cenomanian	Red lutites	85	44	S
PLA29	43.32216	-5.414539	Utrillas Group	Albian-Cenomanian	sand	140	22	NE
PLA30	43.34904	-5.374885	overlaying Utrillas Group	Up. Cretaceous	Grey marly limestone	40	21	NW
PLA31	43.39467	-5.511618	Utrillas Group	Albian-Cenomanian	Red lutites	80	75	S
PLA32	43.3913	-5.519513	Utrillas Group	Albian-Cenomanian	Red lutites	80	65	N
PLA33	43.46404	-5.36582	Buntsandtein	Triassic	Red lutites	110	5	S
PLA34	43.45667	-5.341084	Buntsandtein	Triassic	Red lutites	94	20	N
PLA35	43.47481	-5.217004	Gijón Fm*	**Low. Jurassic**	Grey marls	164	3	E
PLA36	43.51315	-5.267323	Vega Fm*	**Up. Jurassic**	Red sandstones	100	26	N
PLA37	43.50878	-5.271063	Tereñes Fm*	**Up. Jurassic**	Red and grey limestones and clays	98	31	N
PLA38	43.50687	-5.269632	Vega Fm*	**Up. Jurassic**	Red sandstones	40	7	S
PLA39	43.53311	-5.294028	Lastres Fm*	**Up. Jurassic**	Grey sandy marls	125	20	N
PLA40	43.53383	-5.374841	Gijón Fm*	**Low. Jurassic**	Grey limestones and marls	46	27	SE

TABLE II. Average (av.) and standard deviation (stdev) values for all sites: Km (mean susceptibility value), L: k_{max}/k_{min}; F: k_{int}/k_{min}, P: anisotropy degree, Pj: corrected anisotropy degree and T: shape parameter (Jelinek, 1981)

Site	Km av. e-6	Km stdev e-6	L av.	L stdev	F av.	F stdev	P av.	P stdev	Pj av.	Pj stdev	T av.	T stdev
BON01	-5.08	3.6	1.0119	0.013	1.026	0.033	10.47	0.045	1.047	0.046	-0.006	0.309
BON02	11.63	3.476	1.007	0.002	1.006	0.002	1.013	0.003	1.013	0.003	-0.096	0.218
BON03	73.96	6.55	1.003	0.001	1.027	0.002	1.03	0.003	1.033	0.003	0.786	0.078
BON04	34.19	4.603	1.001	0.001	1.002	0.001	1.003	0.001	1.003	0.001	0.085	0.427
BON05	303.1	154.5	1.014	0.012	1.037	0.019	1.052	0.025	1.054	0.026	0.335	0.41
BON06	24.96	5.56	1.004	0.002	1.040	0.007	1.045	0.007	1.050	0.008	0.814	0.094
BON07	165.4	28.88	1.001	0.001	1.001	0.001	1.002	0.001	1.002	0.001	0.239	0.416
BON08	90.39	58.57	1.005	0.003	1.014	0.009	1.019	0.008	1.02	0.01	0.454	0.367
BON09	71.57	15.27	1.014	0.007	1.015	0.006	1.029	0.008	1.03	0.008	0.045	0.367
BON10	133.9	29.47	1.034	0.005	1.022	0.009	1.057	0.009	1.058	0.009	-0.220	0.18
BON11	55.39	10.72	1.014	0.01	1.02	0.011	1.034	0.013	1.036	0.012	0.184	0.55
PLA01	4107	963	1.008	0.004	1.043	0.007	1.052	0.009	1.056	0.009	0.681	0.15
PLA02	180.1	78.49	1.008	0.003	1.014	0.01	1.022	0.011	1.023	0.012	0.198	0.265
PLA03	147.5	59.95	1.01	0.006	1.018	0.007	1.028	0.008	1.029	0.008	0.300	0.309
PLA04	162.8	77.16	1.007	0.006	1.029	0.014	1.037	0.012	1.04	0.013	0.499	0.563
PLA05	227.2	94.7	1.003	0.001	1.005	0.003	1.008	0.003	1.009	0.003	0.126	0.46
PLA06	161.1	24.74	1.004	0.006	1.005	0.006	1.009	0.012	1.009	0.012	0.299	0.368
PLA07	143.6	73.77	1.01	0.009	1.029	0.04	1.039	0.042	1.042	0.048	0.226	0.404
PLA08	161.6	48.5	1.008	0.003	1.032	0.021	1.04	0.02	1.042	0.024	0.553	1.94
PLA09	155.7	38.13	1.007	0.005	1.042	0.011	1.05	0.011	1.054	0.012	0.692	0.277
PLA10	43.79	20.72	1.011	0.009	1.095	0.055	1.107	0.054	1.119	0.063	0.729	0.368
PLA11	89.98	35.29	1.01	0.005	1.005	0.002	1.015	0.004	1.015	0.004	-0.276	0.491
PLA12	108.5	48.68	1.008	0.005	1.017	0.012	1.025	0.016	1.025	0.017	0.287	0.203
PLA13	69.54	27.61	1.011	0.007	1.02	0.014	1.031	0.015	1.033	0.016	0.252	0.43
PLA14	51.03	29.47	1.024	0.019	1.1	0.08	1.127	0.102	1.136	0.109	0.547	0.197
PLA15	38.51	14.93	1.003	0.003	1.009	0.005	1.013	0.05	1.013	0.006	0.464	0.423
PLA16	10.22	5.203	1.014	0.013	1.015	0.013	1.03	0.024	1.03	0.024	0.066	0.347
PLA17	35.05	10.72	1.006	0.006	1.009	0.003	1.015	0.003	1.015	0.003	0.188	0.265
PLA18	86.56	19.16	1.004	0.003	1.010	0.004	1.015	0.003	1.015	0.004	0.398	0.355

TABLE II. Continued

Site	Km av. e-6	Km stdev e-6	L		F		P		Pj		T	
			av.	stdev	av.	stdev	av.	stdev	av.	stdev	av.	stdev
PLA19	39.97	19.55	1.013	0.006	1.021	0.008	1.034	0.012	1.034	0.013	0.237	0.17
PLA20	84.2	49.75	1.015	0.004	1.023	0.008	1.038	0.008	1.038	0.008	0.200	0.198
PLA21	68.81	24.44	1.01	0.004	1.01	0.004	1.02	0.005	1.021	0.005	-0.049	0.294
PLA22	83.87	22.38	1.004	0.002	1.007	0.004	1.011	0.003	1.012	0.003	0.180	0.452
PLA23	67.74	13.8	1.024	0.015	1.03	0.013	1.054	0.024	1.055	0.024	0.148	0.293
PLA24	68.87	15.16	1.024	0.014	1.032	0.015	1.057	0.027	1.058	0.027	0.138	0.233
PLA25	71.06	33.08	1.01	0.004	1.008	0.006	1.018	0.006	1.019	0.006	-0.132	0.398
PLA26	173.5	88.77	1.045	0.045	1.106	0.113	1.159	0.151	1.166	0.16	0.306	0.427
PLA27	43.72	14.62	1.005	0.06	1.009	0.008	1.014	0.009	1.015	0.01	0.192	0.555
PLA28	125.9	11.44	1.004	0.003	1.018	0.007	1.021	0.005	1.023	0.006	1.023	0.006
PLA29	41.81	32.53	1.012	0.005	1.018	0.021	1.03	0.023	1.031	0.025	0.048	0.347
PLA30	45.63	11.37	1.008	0.004	1.018	0.009	1.026	0.01	1.027	0.01	0.311	0.388
PLA31	131.9	52.83	1.014	0.003	1.022	0.006	1.036	0.009	1.036	0.009	0.217	0.127
PLA32	23.9	8.09	1.006	0.003	1.013	0.009	1.02	0.011	1.02	0.011	0.316	0.26
PLA33	177.2	37.94	1.008	0.003	1.047	0.01	1.055	0.011	1.06	0.012	0.711	0.115
PLA34	103.3	14.87	1.007	0.002	1.027	0.013	1.034	0.013	1.036	0.015	0.536	0.149
PLA35	84.27	28.78	1.006	0.008	1.006	0.007	1.012	0.013	1.012	0.014	0.135	0.137
PLA36	77.1	13.22	1.009	0.009	1.018	0.01	1.027	0.01	1.029	0.011	0.326	0.453
PLA37	132.7	105.4	1.007	0.004	1.022	0.013	1.029	0.012	1.031	0.014	0.504	0.29
PLA38	200.5	63.62	1.005	0.002	1.028	0.009	1.032	0.01	1.035	0,11	0.689	0.156
PLA39	113.1	16.77	1.004	0.001	1.035	0.008	1.039	0.009	1.043	0.01	0.787	0.074
PLA40	35.87	11.64	1.006	0.004	1.014	0.012	1.021	0.011	1.022	0.013	0.252	0.474

TABLE III. Average of the orientation of the magnetic ellipsoids for every site After Bedding Borrection (ABC). N: number of samples used, N: total number of samples. $K_{max\ (int,\ min)}$ dec: declination of the $K_{max\ (int,\ min)}$, inc: inclination of the $K_{max\ (int,\ min)}$, confidence ellipse for the average. All calculations are from Anisoft5

Site			ABC Kmax		confidence	Kint		confidence	Kmin		confidence
	n	N	D	I	ellipses	D	I	ellipses	D	I	ellipses
BON01	6	6	135	20	17.6//4.8	243	40	54.1/14.5	25	43	54//8.5
BON02	9	9	66	41	30.9/16	263	48	51.2/22.8	163	9	49.4/16
BON03	8	8	139	12	16.2/4.3	48	4	16/4.4	302	77	5.3/3.8
BON04	8	8	345	7	17.7/16.5	92	48	42.6/17.3	258	41	42.6/15.7
BON05	7	7	78	19	16.5/13.2	290	68	13.7/5.7	172	11	16.6/6.6
BON06	12	12	270	2	63.5/7.7	180	15	63.5/11.3	7	75	13.2/7.1
BON07	8	8	73	7	51.9/14.3	172	48	51.2/19.2	337	41	24.3/14.1
BON08	8	8	101	2	29.7/5.8	11	1	29.7/12	264	88	13/6.3
BON09	9	9	269	6	15.1/5.7	360	6	22.4/9.5	136	82	19.7/6.2
BON10	7	7	99	5	8.3/5.5	190	13	16.5/7.9	347	76	16.6/5.6
BON11	8	8	262	6	32/28.2	354	19	34.4/11.9	156	70	29.2/16.8
PLA01	16	16	**215**	**5**	23.5/6.1	310	13	24.7/12.8	105	76	104.6/75.7
PLA02	13	13	**152**	**9**	35.9/15.9	62	15	37.9/14.9	313	80	21.4/15.8
PLA03	16	16	**205**	**10**	31.3/16.7	295	1	33/18.5	33	80	23.4/15.1
PLA04	16	16	300	0	38.9/14.7	210	0	39.7/24.7	44	89	27.1/15.4
PLA05	15	15	356	71	54.1/18.3	257	3	54.5/22	166	18	26/18
PLA06	15	15	277	3	23.9/5.1	180	65	49.4/23.8	9	25	49.4/5
PLA07	13	13	**112**	**10**	27.9/7.4	206	25	35.7/25	1	63	34.6/10.2
PLA08	15	16	**305**	**8**	23.4/9.8	36	6	22.8/9.8	163.3	80	19.6/7.7
PLA09	16	16	**294**	**6**	10.8/4	203	9	12.8/7.5	58	79	10.5/4.4
PLA10	10	10	**286**	**3**	25/8.1	17	6	30.6/24.4	171	83	30.5/6.1
PLA11	13	13	**116**	**3**	6.3/5.6	207	5	39.7/4	354	84	39.6/5.6
PLA12	16	16	**280**	**7**	30.7/12.5	190	12	33.9/19.8	40	76	26.6/11.9
PLA13	17	17	**126**	**2**	38.9/16	217	12	40.5/18	27	78	27.1/12
PLA14	14	16	178	36	31/11	78	37	30/16	331	51	21/10
PLA15	14	14	26	1	63/8	116	11	63/12	293	79	13/10
PLA16	11	11	105	65	43/40	358	8	57/41	265	24	61/25
PLA17	9	9	227	8	23/20	318	9	24/13	96	79	22/10
PLA18	12	12	52	9	14.3/5.2	317	29	16.3/12.6	157	59	16/7.8
PLA19	12	12	33	6	8.7/4.4	124	11	8.7/7.2	275	77	8/3.4

TABLE III. Continued

Site	n	N	ABC Kmax D	I	confidence ellipses	Kint D	I	confidence ellipses	Kmin D	I	confidence ellipses
PLA20	12	12	230	9	9.8/7.6	139	4	11.5/6.7	26.4	80	9.1/7.6
PLA21	9	9	312	48	26/10	219	3	34/22	162	42	32/14
PLA22	12	12	80	1	22/8	170	54	22/11	349	36	13/8
PLA23	14	14	102	6	36/17	196	34	45/34	3	55	44/15
PLA24	10	14	101	2	19/5	193	34	39/14	9	56	39/7
PLA25	11	11	243	6	17/9	333	0	18/16	66	84	18/7
PLA26	11	11	17	12	58/13	112	22	58/6	261	64	16/4
PLA27	13	13	248	5	29/12	248	5	28/19	23	83	19/13
PLA28	14	14	177	5	16/10	268	16	21/10	70	73	22/14
PLA29	13	13	257	16	45/17	353	19	39/26	128	65	39/20
PLA30	16	16	71	11	47.2/11.6	162	6	47.2/7.9	282	77	12(8
PLA31	11	11	269	34	11.6/4.8	168	15	17.9/6.9	58	52	17.7/9.2
PLA32	21	21	251	23	48.6/10.5	350	19	48.8/17.9	116	60	19.4/10.9
PLA33	17	17	341	2	29.3/3	71	3	29.3/4.5	220	86	4.6/3
PLA34	10	10	13	4	24.4/6.6	103	5	24.2/9	242	84	11.5/4.6
PLA35	34	34	348	4	15.3/9	79	12	41.7/11.7	240	77	41.1/9.4
PLA36	15	15	135	5	54.4/7.1	45	1	54.4/14.3	306	85	14.9/7.9
PLA37	25	26	192	7	26.5/7.5	101	10	26.5/11.4	315	78	11.6/7.1
PLA38	23	23	30	6	32.9/6.4	300	3	32.9/12.8	182	84	13.4/5.4
PLA39	20	20	166	4	22.8/4.5	256	1	22.6/4.8	357	86	5.5/4.6
PLA40	20	20	335	31	28.1/21.9	66	1	33.9/21.9	158	59	31.8/18.3